國立臺灣大學生命科學院生化科學研究所

碩士論文

Graduate Institute of Biochemical Sciences
College of Life Science
National Taiwan University

Master Thesis

探討老鼠普立昂蛋白進行結構轉變時三段阿法螺旋扮演的角色

Exploring the role of three α-helices on the structural conversion of mouse prion protein

羅瑋霖
Wei-Lin Luo

指導教授：陳佩燁 博士
Advisor: Rita Pei-Yeh Chen, Ph.D.

中華民國 101 年 7 月
July, 2012

誌謝

還記得，準備研究所考試的認真，在台大生化所榜單上看到自己名字時的快樂，這些好像都是昨天才發生的事。現在，畢業的時刻來臨，興奮中不免也帶些惆悵。從高中到研究所，我都是在台北求學，桃園到台北的火車，不知道搭過幾千趟。一轉眼，十年就過去了，而人生的列車也到了開往下一站的時候。

這篇論文能夠順利地完成，首先要感謝我的指導教授陳佩燁老師。從老師身上學到了很多，包括對研究的熱情，如何去驗證自己的想法以及從既有結果作出的邏輯推演等等。這些不僅僅是實驗上的，也可以應用到未來的任何層面，我認為就是兩年來最大的收穫。感謝清大的江昀緯老師和蔡佳容學姊，幫助我進行 ESR 實驗的偵測以及結果分析，對於完成論文有很大的貢獻。也要感謝黃人則老師、金之彥老師和陳炳宇老師在百忙中抽空來當我的口試委員，也提供了非常寶貴的意見。

謝謝 504 實驗室的大家。論文是從桑傑學長的部分延伸下去的，其中的實驗也幾乎都是他教我的，非常感謝他。信良學長在儀器方面給了我很多建議，而且對於時事也非常有見解。陸逸麟博士教導了實驗的態度和技巧。Biswanath 博士對於實驗也給了很多幫助和建議。不管任何大小事，找苔言學姊就對了，都能得到很好的解答。惠玲學姐和忠諭學長也十分關心我，提供我非常多幫助。林辰學長，芝韻學姐和綺珍學姐帶我熟悉了實驗室，也都很照顧我。柏廷學長、昭隆和心彥人都很好，和他們聊天是很快樂的事。兩位學弟，楊哲和晏溥給實驗室帶來許多歡樂與活力。

實驗雖然繁忙，但是朋友們一起歡笑的時光卻足以抵銷，謝謝你們。又權是我研究所最好的朋友，從開學第一天便認識了，每天苦惱晚餐種類和互講垃圾話是排解壓力最好的方法。施施、峻豪、Gino、Thisway、碩甫、昕永和文瑄一起在籃球場打球的時光，也是十分熱血痛快。絹姐、明媛、妃儀、政諭、5-1 等人都是研究所中一起奮鬥的朋友。廢物團的嘿嘿、艾可、巴辣、小寶、麻吉和魯曼一起聚

會的時光，實在是非常北爛有趣，總是充滿著歡笑。杰哥、勇佐都是好戰友，我們一起在電玩中征戰四方。

感謝爸爸和媽媽，提供我一切需要，支持我做的決定，沒有你們的幫助和關愛，我也不會有今天的成果。謝謝鈺婷，幫我修改論文的文法，讓我能順利完成。謝謝羽珊，跟我分享家中大小事，在我不在家時，陪伴著媽媽。當然還要謝謝我的女友宛余，雖然上研究所之後，我們相聚的時間變少，但還是溫柔的支持我，跟兔子喜歡吃紅蘿蔔一樣，讓我在人生旅途中並不孤單。

謹將此論文獻給所有關心我、幫助我的人，謝謝你們!

中文摘要

普立昂疾病是一類具傳染力且致命的神經退化性疾病，會侵襲中樞神經系統造成人類或動物腦組織產生海綿狀的病變。其致病物質為錯誤折疊的普立昂蛋白(PrP^{Sc})，有容易聚集和傳染的特性。細胞中正常的普立昂蛋白(PrP^{C})是 α 螺旋為主的結構，會轉變成以 β 摺板為主的致病性普立昂蛋白(PrP^{Sc})，而聚集成易沉澱的澱粉樣類纖維構造。這種不正常的結構轉變便是造成細胞毒性的主要原因。但是目前我們仍然不清楚普立昂疾病結構轉變的過程和致病機制。本實驗室在先前研究中發現雙硫鍵被移除的重組普立昂蛋白，可以在中性環境下進行自發性的結構轉變。它可以轉變成β寡聚體或者澱粉樣類纖維構造。為了探討不同區域的資訊，在這項研究中，我們先分別標定在普立昂蛋白的三個 α 螺旋上。接著，將標定的普立昂蛋白進行結構轉變，包括自發性結構轉變，形成β寡聚體以及形成澱粉樣類纖維構造。我們利用圓二色光譜和電子自旋共振(ESR)圖譜等技術來探討這些區域有無參與結構轉變。在自發性的結構轉變中，我們發現整體結構變得比較鬆散。另外，在β寡聚體的結構時，helix 1 和 helix 2 的結構會部分解開，而helix 3 可能維持在穩定的結構中。最後，在澱粉樣類纖維構造中，我們發現helix 3 的分子間距離只有 1 奈米，但仍然需要進一步實驗來確認 β 摺板為主結構是由哪一區域轉變成的。

關鍵字：普立昂疾病、錯誤折疊、結構轉變

Abstract

Transmissible Spongiform Encephalopathies (TSE), also called prion diseases are infectious neurodegenerative disorders. The key molecular event in the pathogenesis of prion diseases is the conformational conversion of a cellular prion protein, PrP^{C}, into a misfolded form, PrP^{Sc}. The α→β conformational transition leads to protein aggregation and the formation of toxic amyloid fibrils. However, the mechanism of protein misfolding and the pathogenic pathway are still unclear. In our lab's previous study, we found that the disulfide-deleted mouse PrP could undergo a spontaneous structural conversion under native condition from the native α-helical structure to β-oligomers, amorphous aggregate, even amyloid fibrils. Here, we made spin-labeling on each of three helices of mouse prion protein individually and combined circular dichroism spectroscopy and electron spin resonance (ESR) spectroscopy to investigate the structural conversion process. Our study illustrated that helix 1 and helix 2 were partially unfolded when converted into soluble β-structures. On the other hand, spin labeled on helix 3 showed slow mobility, suggesting that the local environment of that spin is in an ordered state. Moreover, when the helix3-labeled protein was transformed into amyloid fibrils, the spin-labeled fibrils showed intermolecular spin interaction with a distance of 10 Å.

Keywords: Prion disease, misfolding, structural conversion

Abbreviations

AD	Alzheimer's disease
APS	ammonium persulfate
BSE	bovine spongiform encephalopathy
CD	circular dichroism
CJD	Creutzfeldt-Jacob disease
CV	column volume
CWD	chronic wasting disease
DMSO	dimethyl sulfoxide
EDTA	ethylenediaminetetraacetic acid
EPR	electron paramagnetic resonance
ESI-TOF	electrospray ionization - time of flight
ESR	electron spin resonance
FFI	fatal familial insomnia
FTIR	Fourier-transform infrared spectroscopy
GdnHCl	guanidium hydrochloride
GPI	glycosylphosphatidylinositol
GSS	Gerstmann-Sträussler-Scheinker syndrome
HD	Huntington's disease
HPLC	high performance liquid chromatography
IMAC	immobilized metal affinity chromatography
IPTG	isopropyl β-D-1-thiogalactopyranoside
LB	lysogeny broth or Luria-Bertani broth

MS	mass spectrometry
MTSSL	(1-oxyl-2,2,5,5-tetramethylpyrroline-3-methyl)methanethiosulfonate
NaOAc	sodium acetate
NMR	nuclear magnetic resonance
PBS	phosphate buffered saline
PCR	polymerase chain chain
PD	Parkinson's disease
PK	proteinase K
PrP	prion protein
PrP^{C}	cellular PrP isoform
PrP^{Sc}	pathogenic (scrapie) PrP isoform
RT	room temperature
SDSL	site-directed spin labeling
SDS-PAGE	sodium dodecyl sulfate – polyacrylamide gel electrophoresis
SV-AUC	sendimentation velocity – analytical ultracentrifugation
TB	teriffic broth
TCEP	*tris*(2-carboxyethyl)phosphine
TEM	transmission electron microscope
TEMED	N,N,N',N'-tetramethylethylenediamine
TFA	trifluoroacetic acid
ThT	thioflavin T
Tricine	N-[tris(hydroxymethyl)methyl]glycine
TSE	transmissible spongiform encephalopathy
UV	ultraviolet

A (Ala)	alanine
C (Cys)	cysteine
D (Asp)	asparatate
N (Asn)	asparagine
Q (Gln)	glutamine
S (Ser)	serine

Contents

Figure contents

Chapter 1 Introduction

1.1 Introduction to prion disease

Prion diseases (or transmissible spongiform encephalpathies, TSE) are a group of fatal neurodegenerative disorders that affect numerous mammalian species, including kuru, sporadic Creutzfeldt-Jakob disease (sCJD), familial CJD (fCJD), iatrogenic CJD(iCJD), Gerstmann-Stra¨ussler-Scheinker disease (GSS), fatal insomnia (FI), and new variant CJD (vCJD) in human, bovine spongiform encephalopathy (BSE) in cattle, scrapie in sheep and chronic wasting disease (CWD) in deer and elk (Table 1). The neurodegenerative diseases contain Huntington's disease (HD), Parkinson's disease (PD), Alzheimer's disease (AD) and so on. A unique feature of prion diseases is that they are transmissible and able to across species. After a protracted incubation period, patients display clinical symptoms of progressive motor dysfunction, cognitive impairment, and cerebral ataxia. The brains of diseased individuals show characteristic spongiform degeneration, astrogliosis and accumulation of misfolded protein deposits (Cobb & Surewicz, 2009; Prusiner, 1998). All forms of prion disease are progressive and ultimately fatal. Currently, there are no treatments that have been shown to halt progression or to reverse the disease.

Table 1 TSEs in different animals. (Imran & Mahmood, 2011)

Animal prion diseases			
Disease	**Host**	**Etiology**	**Year of Description**
Scrapie	Sheep, Goats	Infection with Prions of unknown origin	1732
TME	Mink	Infection with Prions of either sheep or cattle origin	1947
CWD	Cervids	Infection with Prions of unknown origin	1967
BSE	Cattle	Infection with Prions of unknown origin	1986
EUE	Nyala, Kudu	Infection with Prions of BSE origin	1986
FSE	Cats	Infection with prions of BSE origin	1990
NHP	Lemurs	Infection with Prions of BSE origin	1996
Human prion diseases			
Disease	**Host**	**Etiology**	**Year of Description**
Kuru	Human	Ritualistic Cannibalism or "Transumption"	1900s
sCJD	Human	Spontaneous $PrP^{C} \rightarrow PrP^{Sc}$ conversion or somatic mutation	1920
fCJD	Human	Mutations in *PRNP*	1924
GSS	Human	Mutations in *PRNP*	1936
iCJD	Human	Infection with Prions of human origin by cadaveric corneal grafts, hGH or dura mater	1974
FFI	Human	*PRNP* haplotype 178N-129M	1986
vCJD	Human	Infection with Prions of BSE origin	1996
sFI	Human	Spontaneous $PrP^{C} \rightarrow PrP^{Sc}$ conversion or somatic mutation	1999
VPSPr	Human	Spontaneous $PrP^{C} \rightarrow PrP^{Sc}$ conversion or somatic mutation	2008

The ancient prion diseases, sheep scrapie, had been reported since early eighteen century in Great Britain. The name "scrapie" comes from the behavior of the infected sheep which tend to scrapie their fleece against trees and bushes. In 1922, the term "Creutzfeldt-Jakob disease" (CJD) was used to describe a human neurodegenerative disease from earlier reports by Creutzfeldt and Jakob (Prusiner, 1998). In 1936, Cull□ and Chelle successfully transferred scrapie from sheep to goats, demonstrating that scrapie was an infectious disease (Cuille & Chelle, 1939). Another human disease, kuru, which was transmitted by ritualistic cannibalism was discovered at Papua New Guinea in 1936 (Steadman, 1980). In 1959, Hadlow pointed out the analogies between

kuru and scrapie in clinical features and pathology (Hadlow, 1959). D. C. Gajdusek confirmed that kuru can be transmitted to chimpanzees in 1966; 2 years later, Gibbs proved the transmission of CJD (Gajdusek et al, 1966; Gibbs et al, 1968).

Since BSE (bovine spongiform encephalopathy, or “mad cow disease”) in cattle was first reported in 1986 in the United Kingdom, it had rapidly evolved into a major epidemic (Wells et al, 1987). More than 180,000 cattle were infected and 4.4 million were slaughtered during the eradication program in Britain (Trevitt & Singh, 2003). It is believed that feeding dairy cows with considerable meat and bone meal (MBM) is the cause of BSE (Wilesmith et al, 1991). MBM is prepared from the offal of many different resources and thus is possibly contaminated with scrapie or other prion diseases. Approximately ten years after BSE epidemic, a new type of human TSE was found in Great Britain and was called variant CJD (vCJD). Compared with sporadic CJD (sCJD), the patients of vCJD were relatively younger, they manifested a predominance of psychiatric symptoms instead of cerebellar ataxia or progressive dementia (Will, 2003). Both epidemiologic and experimental studies indicated that vCJD was resulted from exposure to the contaminated BSE cattle products (Bruce et al, 1997; Will et al, 1996). Figure 1.1 displays the statistical data about BSE and vCJD from 1987 to 2010, showing some correlations between these two prion diseases.

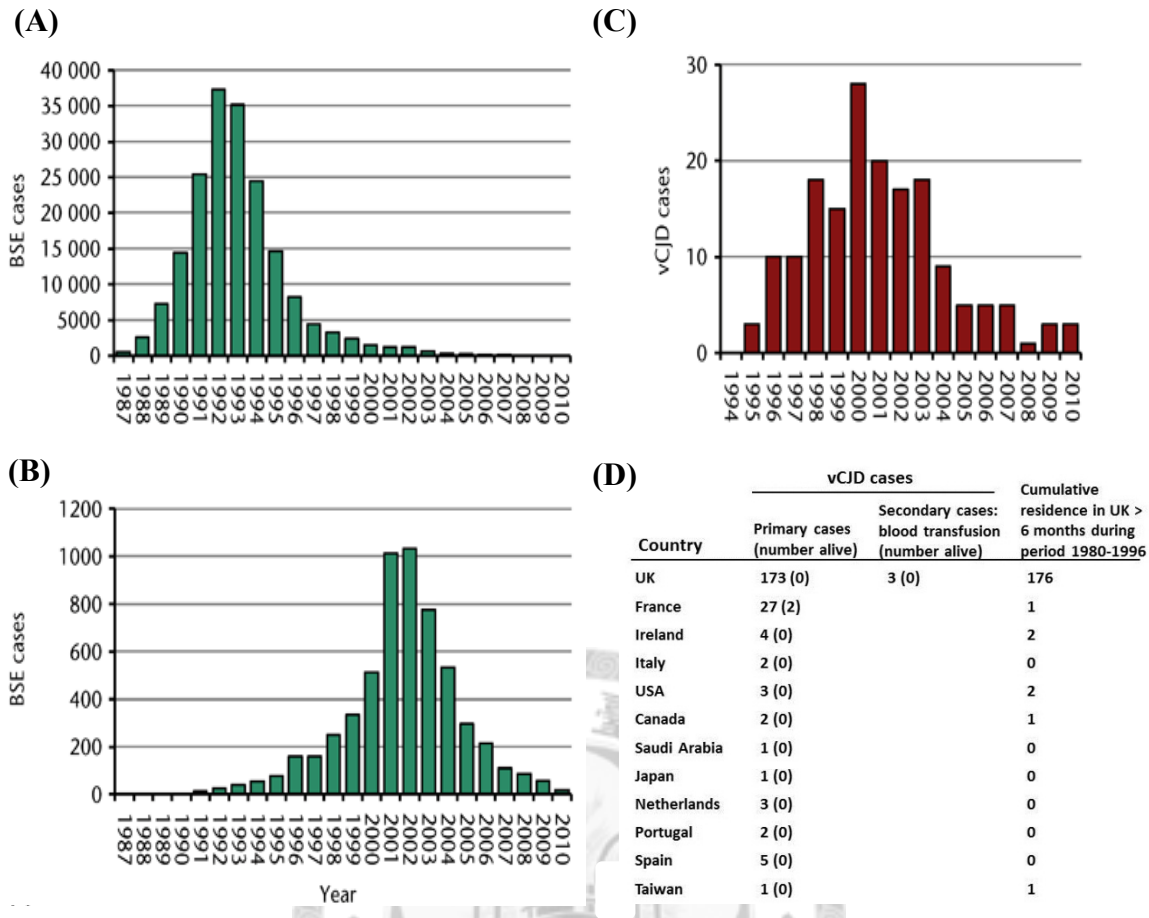

Country	vCJD cases: Primary cases (number alive)	vCJD cases: Secondary cases: blood transfusion (number alive)	Cumulative residence in UK > 6 months during period 1980-1996
UK	173 (0)	3 (0)	176
France	27 (2)		1
Ireland	4 (0)		2
Italy	2 (0)		0
USA	3 (0)		2
Canada	2 (0)		1
Saudi Arabia	1 (0)		0
Japan	1 (0)		0
Netherlands	3 (0)		0
Portugal	2 (0)		0
Spain	5 (0)		0
Taiwan	1 (0)		1

Figure 1.1 BSE and vCJD cases. (A) BSE cases reported in the United Kingdom. (B) BSE cases worldwide excluding the United Kingdom. (C) vCJD cases reported in the United Kingdom. (D) Cumulative vCJD cases in individual countries (current data until July, 2012). Statistical data were obtained from The National Creutzfeldt-Jakob Disease Research & Surveillance Unit (NCJDRSU) (www.cjd.ed.ad.uk). The third US patient with vCJD was born and raised in Saudi Arabia and has lived permanently in the United States since late 2005. According to the US case-report, the patient was most likely infected as a child when living in Saudi Arabia. The case from Japan had resided in the UK for 24 days in the period 1980-1996. (Ryou, 2011)

According to the statistical data until July 2012, there were 224 vCJD cases reported in world-wide. Most of them had resided in U.K more than 6 months during the BSE epidemic period between 1980 and 1996. Unfortunately, only two of the patients had survived until now.

1.2 Protein only hypothesis

The word “prion” stands for “proteinaceous infection particle,” which was named by Prof. Stanley Prusiner (Prusiner, 1982). Since the disease was discovered, there had great debates about the pathogen of prion diseases. Until now, it has been widely accepted that the infectious particles of prion diseases are misfolded proteins. At first, people described the infectious agent as “slow virus” (Rogers et al, 1967). However, Alper and co-workers demonstrated that ionizing radiation and UV did not destroy the infectious material whose size was too small to be a virus (Alper et al, 1967; Alper et al, 1966). In 1967, Griffith proposed that the infectious agent might be a protein (Griffith, 1967). But few researches had been done to test the hypothesis until Prusiner purified the scrapie agent and coined the term prion in 1982 (Prusiner, 1982). After that, more and more researches supported the protein hypothesis. The gene encoding PrP (*PRNP*) was identified in the mammalian genome and the familial prion diseases were all resulted from *PRNP* mutations (Collinge, 2001; Oesch et al, 1985). Furthermore, the strong evidence was provided from transgenic mice. Overexpression mutant *PRNP* in mice produced a transmissible neurodegenerative disorder similar to prion disease (Hsiao et al, 1990). The transgenic knocked out mice (*PRNP*$^{-/-}$) were resistant to scrapie infection without any signs of the disease (Bueler et al, 1993). Moreover, prion-similar infectious materials were generated in vitro with defined components

which further supported for the prion hypothesis (Castilla et al, 2005; Wang et al, 2010).

1.3 Prion infectious conversion

Prion diseases are caused by the misfolded isoform of the prion protein (PrP). Prion proteins have a molecular weight of 33-35 kDa and exist in two isoforms: the nonpathogenic, predominantly α-helical, protease-sensitive, cellular isoform form (PrP^C, C stands for "cellular") and the pathogenic, protease-resistant scrapie-inducing isoform (PrPSc, Sc stands for "scrapie") that is high in β-sheet structure. PrP^{Sc} stimulates native PrP^C to convert into infectious PrP^{Sc} and is further accumulated in the brain which causes neurodegeneration. These two isoforms have identical primary sequence and no different posttranslational modifications have found (Stahl et al, 1993). An apparent decrease in α-helix content and a significant increase in β-sheet content occur during the PrP^C to PrP^{Sc} conversion (Pan et al, 1993). These findings are surprising because they challenge the Affinsen's dogma "one sequence, one structure"(Anfinsen, 1973). Compare to PrP^C, which is protease-sensitive and solubility, PrP^{Sc} shows limited proteinase-resistance and is insoluble in non-denaturing detergent. Limited protease digestion of PrP^{Sc} often produces a smaller, N-terminal-excision protease-resistant core (approximately 142 amino acid), referred as PrP 27–30 (McKinley et al, 1983).

The central molecular event in prion diseases is the self-propagating conformational conversion of PrP^{C} to misfolded form PrP^{Sc}. Despite the mechanism is still unknown, two conceptually different models have proposed for this protein replication process (fig. 1.2). Due to template assistance model, PrP^{Sc} exists as thermodynamically stable but kinetically inaccessible monomer. PrP^{Sc} is a catalytic template that assists PrP^{C} to convert into more stable PrP^{Sc} conformation and the rate-determining step of the process is forming the heterodimer between PrP^{Sc} and PrP^{C} (Prusiner, 1991). While such a mechanism is plausible, there is no experimental evidence for the existence of a stable PrP^{Sc} monomer (Surewicz & Apostol, 2011). In contrast, some reports indicated that aggregation process was intimately associated with prion protein conversion (Morillas et al, 2001; Swietnicki et al, 1999). A much proper model is nucleated polymerization mechanism (Jarrett & Lansbury, 1993). According to this model, the conversion between PrP^{Sc} and PrP^{C} is reversible, but the PrP^{Sc} monomer is less stable. The critical step of structural conversion is forming the oligomeric nucleus which can stabilize PrP^{Sc}. Once the nucleus has been formed, monomeric PrP^{C} could efficiently be added to it and successfully becomes PrP^{Sc}. The nucleation step causes the lag time of spontaneous structural conversion which can be bypassed by adding PrP^{Sc} seeds.

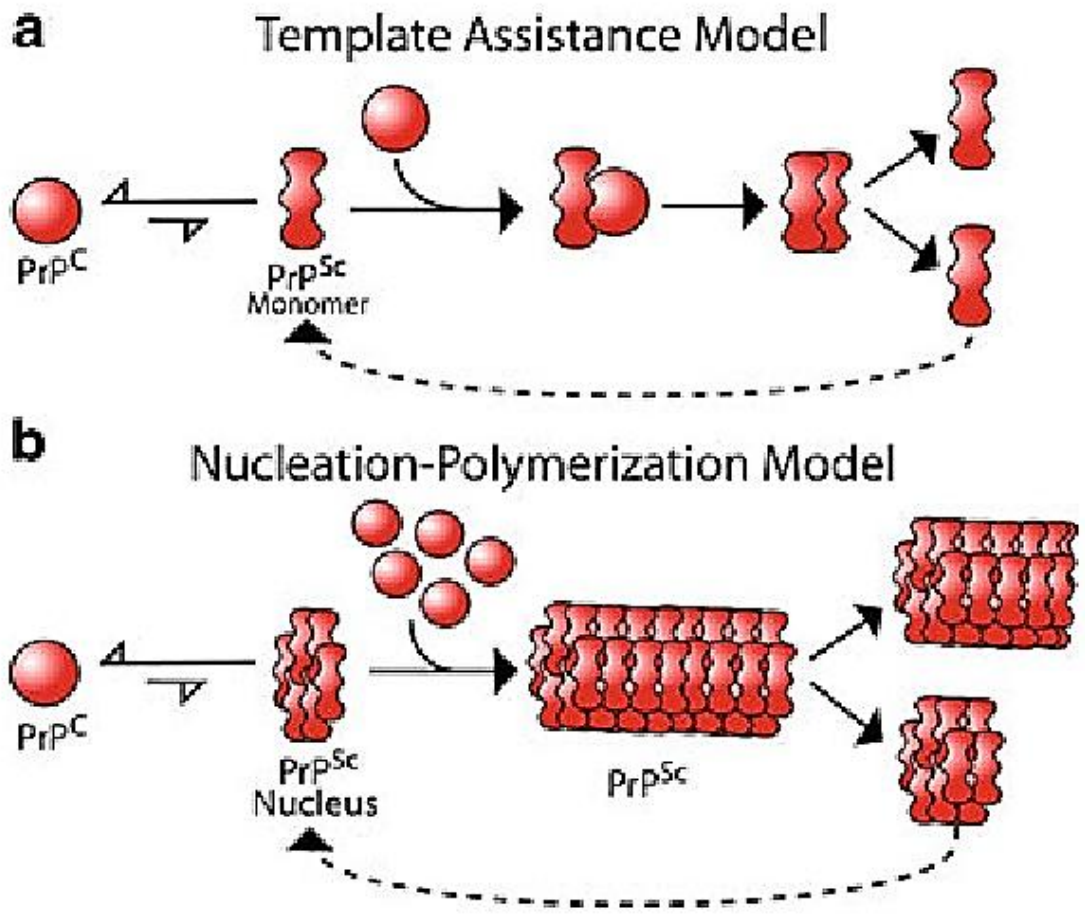

Figure 1.2 Models of prion replication. (A) The template assistance model predicts that a PrP^{Sc} monomer is more stable than PrP^{C}, but is kinetically inaccessible. In the rare event that PrP^{Sc} monomer is created spontaneously (or provided exogenously), it can template the misfolding of another PrP^{C} molecule by direct interaction. The dashed line shows that the newly created PrP^{Sc} monomer can act as another seed to formation of PrP^{Sc}. (B) The nucleation polymerization model predicts that barrier to prion protein conversion is the formation of a nucleus in which the protein adopts a PrP^{Sc}-like structure. The formation of such a low order aggregate is not favored; however, once it has formed, polymerization from a pool of PrP^{C} molecules can take place efficiently. Fragmentation of the polymer increases the number of ends for the recruitment of PrP^{C} monomers. (Surewicz & Apostol, 2011)

1.4 The structural and biological aspect of PrP^C

PrP^C is a glycoprotein which normally attaches to membrane by a glycosyl phosphatidylinositol (GPI) anchor and is highly conversed between mammals. In hamster, PrP is encoded as a 254 amino acids polypeptide. The signal sequences including 22 amino-acids of N-terminal and 23 amino acids of C-terminal are removed during posttranslational modification. Functional PrP^C attaches to cell membrane through a GPI anchor at Ser 231. PrP^C further contains one disulfide bond between Cys 179 and Cys 214, and two N-linked glycosylation sites on Asp 181 and Asp197 (fig 1.3 A).

A highly flexible N-terminal domain and a structural C-terminal domain compose the structure of PrP^C. N-terminal domain contains octapeptide repeats which have the binding ability to many materials such as Cu^{2+}, polyanions, oligonucleotides and nucleic acids (Burns et al, 2002; Caughey & Baron, 2006). The PrP^C structures of different vertebrates including human, cows, sheep and mouse have been solved by Nuclear magnetic resonance (NMR) (López García et al, 2000; Lysek et al, 2005; Riek et al, 1996). These studies reveal a consensus structure composed of three α-helices, two antiparallel β-sheet and one disulfide bond between helices 2 and 3 (fig. 1.3 B).

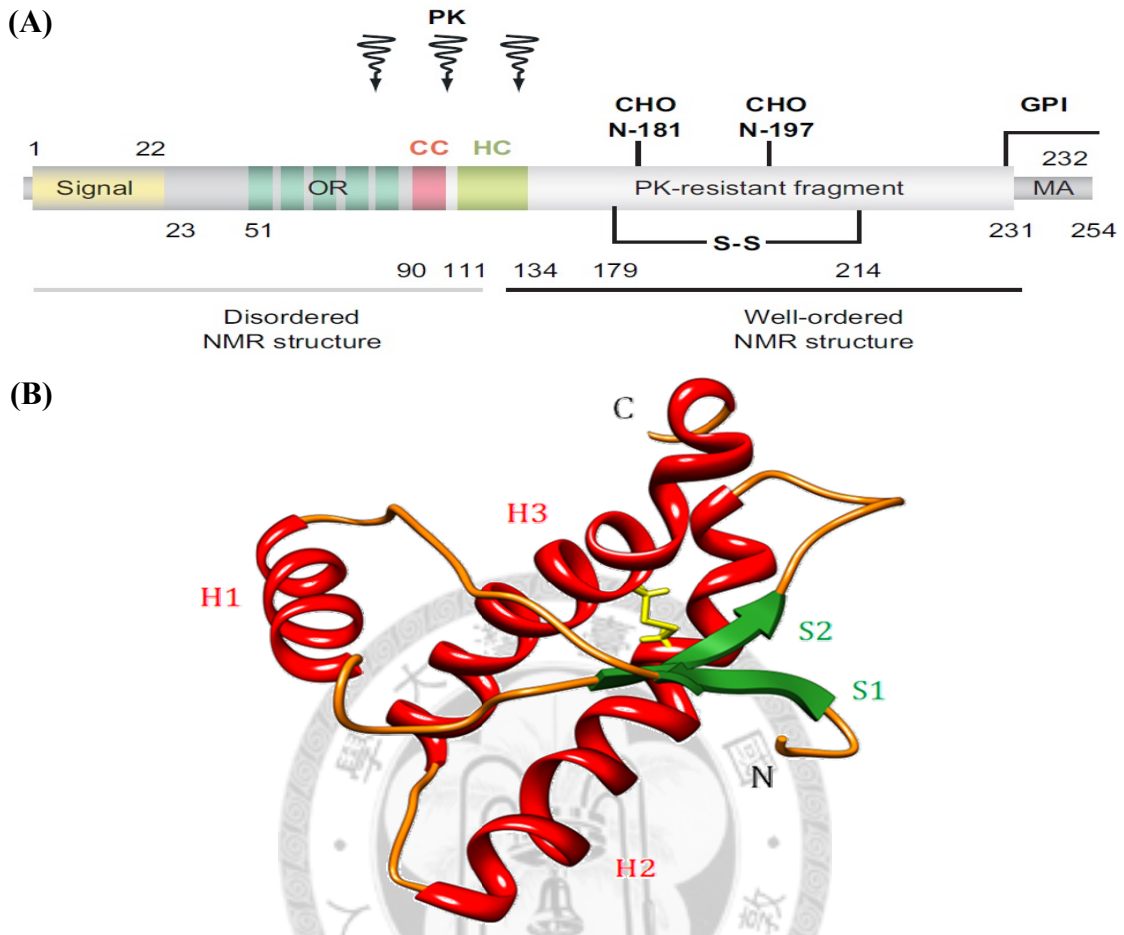

Figure 1.3 The structure of PrP^C. (A) Scheme of the primary structure of the cellular prion protein and its posttranslational modifications. A secretory signal peptide resides at the extreme N terminus. The numbers describe the positions of the respective amino acids. The proteinase K (PK)-resistant core of PrP^{Sc} is depicted in gray; the approximate cutting site of PK within PrP^{Sc} is indicated by arrows. OR, octapeptide repeats; CC (*pink*), charged cluster; HC (*green*), hydrophobic core; S-S, single disulfide bridge; MA, membrane anchor region; GPI, glycosyl phosphatidyl inositol; CHO, facultative glycosylation sites. (Aguzzi et al, 2007) (B) NMR structure of mouse PrP C-terminal (121-231). 3D structure reveals three α-helices (H1, H2 and H3), two anti-parallel β-sheets (S1 and S2) and one disulfide bond between helix 2 and helix 3.

PrP^C ubiquitously exists around peripheral tissues including lung, heart, kidney, pancreas, testis, white blood cells and platelets (Bendheim et al, 1992; Perini et al,

1996). But highly expression is found in neuron cells (Kretzschmar et al, 1986). However, the function of PrP^{C} is still unclear, although several studies propose that it has variant functions. For example, PrP^{C} is related to formation, maintenance and functions of synapses (Collinge et al, 1994; Kanaani et al, 2005). PrP^{C} is a membrane glycoprotein, suggesting a role in cell signaling or adhesion (Málaga-Trillo et al, 2009; Spielhaupter & Schätzl, 2001). Moreover, prion protein possesses Cu^{2+}-binding ability, indicating that it may play a role in copper homeostasis (Brown et al, 1997; Davies & Brown, 2008). Interestingly, no obvious developmental or behavioral abnormality were noted in PrP knockout mice (Bueler et al, 1992). However, recently works also suggested that PrP-deleted adult mice displayed some hippocampal-dependent spatial memory deficits and had impaired peripheral myelin maintenance (Bremer et al, 2010; Criado et al, 2005).

1.5 Different models of PrP^{Sc}

Determining the structural features that differentiate between PrP^{C} and PrP^{Sc} will provide an important insight into the pathogenic conversion mechanism and the therapy of prion disease. Structural properties of PrP^{Sc} remain poorly characterized despite decades of research. Getting atomic structure by NMR and X-ray diffraction is very difficult because PrP^{Sc} is insoluble and easily aggregate. However, we found that the

structural conversion from PrP^{C} to PrP^{Sc} with decrease in α-helical secondary structure (40%→30%) and striking increase in β-sheet contents (3%→ 43%) as measured by Fourier transform infrared (FTIR) and circular dichroism (CD) (Pan et al, 1993).

In the absence of direct experimental data, the structures proposed for PrP^{Sc} are largely based on modeling efforts, which will be introduced in the following contents. According to the electron density from electron micrographs of two-dimensional PrP 27-30 rods, β-helical model was proposed and shown in fig. 1.4 A (Govaerts et al, 2004; Wille et al, 2002). β-helical model presumes that residues 89-175, which include native β-stands and helix 1 of PrP^{C}, are in left-handed β-helix conformation. The β-helical domains of PrP associate into trimers, where the α-helices 2 and 3 are largely preserved as in the native structure. And oligosaccharides decorate the outside of the trimers. The β-helical trimers are stacking on each other to form an extended β-sheet core of fibril. This model is compatible with the X-ray fiber diffraction of prion rods (Wille et al, 2009), and is also consistent with the amyloid core structure of fungal prion (Wasmer et al, 2008). However, we still lack of experimental data to demonstrate that β-helical structure is indeed present in PrP^{Sc}. Another is β-spiral model, which was derived from molecular dynamics simulations using the PrP^{C} monomer as a starting point (DeMarco & Daggett, 2004). In this model, all three helices retain their native

structures. During the structural conversion, a longer β-sheet is formed by two native β-strands and two new β-strands coming from the loop between strand 1 and helix 1 (fig. 1.4 B). The β-spiral model proposes that the PrP can form intermolecular β-sheet by these new β-strands during polymerization. In order to fit the electron density from two-dimensional electron micrographs, the basic subunit is predicted as trimers. The new β-sheets are "spiral" around fibril axis at 45° pitch in the stacked assembly of the trimers becoming PrP protofibril. However, β-spiral model could not account for the cross-β diffraction pattern found for PrP^{Sc}, implying that this may be an intermediate state in further transformation into PrP^{Sc}-like amyloid (Surewicz & Apostol, 2011). The third one is two-rung model, which is based on left hand β-helical model and is further refined by molecular dynamics simulations and modeling. Two-rung model suggests that PrP region with the highest β-helical propensity (residues 105–143) can fold in just two rungs of a left-handed β-helix (Langedijk et al, 2006). The first β-helix rung is composed of residues 125-143 and the second β-helix rung is composed of residues 106-124 (fig. 1.4 C). The two rungs of β-helix can give the growing fibril in a tight packing at the periphery of a trimeric β-helix. Compare to β-helical model, both models show trimeric β-helix, but all three α-helices are retained in the two-rung model. The fourth model is domain-swapping model. This model results from the crystal structure of human PrP 90-231 in dimer form at 2 Å resolution (Knaus et al, 2001).

The dimer is come from three-dimensional swapping of the C-terminal helix 3 and rearrangement of the disulfide bond (fig. 1.4 D). Recently, another paper found that only the disulfides that tethered subdomain B1-H1-B2 to subdomain H2-H3 could prevent PrP conversion in vitro (Hafner-Bratkovic et al, 2011). This report further supported the domain-swapping model.

On the other hand, rPrP amyloid fibrils forming in vitro with different techniques also provide some structural information. The parallel, in-register β-structure has been found experimentally for rPrP amyloid fibrils and is consistent with following biophysical methods (fig. 1.5 A). In contrast to the models described above, the parallel, in-register β-structure indicates that C-terminal is involved in structural transition and no native α-helices are present in PrP^{Sc} conformation. Amyloid fibrils formed from human rPrP90–231 were combined with site-directed spin labeling (SDSL) and electron spin resonance spectroscopy (ESR). The distance measurements by SDSL revealed that residues within the ~160–220 core region forms single-molecule layers that stacked on top of one another with a parallel and in-register alignment of β-strands (Cobb et al, 2007). In addition, hydrogen/deuterium exchange coupled with mass spectrometry (HXMS) was used to study amyloid core. This method is particularly well suited for studying amyloid fibrils because the amide protons in the

β-sheet core of fibrillar aggregates are resistant to the exchange. The most highly exchange-protected region in huPrP 90-231 fibrils is starting from residue 169 and extending to at least residue 213 (Lu et al, 2007). Therefore, the HXMS data confirmed that C-terminal is involved in amyloid core. The parallel, in-register β-structure is also confirmed by solid-state NMR experiments of recombinant Syrian hamster PrP23-231 amyloid fibrils. Solid-state NMR showed that these fibrils contain in-register parallel β-sheets and that the structurally ordered fibril core includes the C-terminal segment, approximately residues 175-225, which includes the second and third α-helices of monomeric PrP (Tycko et al, 2010). Moreover, recombinant huPrP 90-230 fibrils combined with solution NMR also showed consistent results. Solution NMR data suggested that residues 145–223, including all three α-helices, forming the rigid core of the fibrils (Kumar et al, 2010). Figure 1.5 B presents amyloid core investigated by different experimental methods.

Interestingly, prion peptides from disordered region could also form fibrils in vitro and the amyloid core region investigated by solid state NMR was distinct from the above experiments. For example, solid state NMR experiments indicated that the ordered β-core in fibrils formed by C-terminally human PrP (huPrP23–144) mapped to residue 112–141 (Helmus et al, 2008). Another solid state NMR study revealed that

human PrP(106–126) formed in-register parallel β sheets within the mature fibril (Walsh et al, 2009). Hamster PrP 109-122 peptide could form amyloid fibrils as well, but solid state NMR showed that the conformation was antiparallel β sheets (Lee et al, 2008). In addition, in-register parallel β-sheet was found from human PrP 127-147 fibrils and residue 137 may generate a twist between adjacent peptide strands (Lin et al, 2010). Furthermore, Eisenberg and coworkers have found that small peptides from amyloidogenic proteins, including PrP, can form a variety of parallel and antiparallel structures (Sawaya et al, 2007). These structures are arranged in tightly self-complementing β-sheets and are called steric zippers (Nelson et al, 2005) (fig. 1.5 C).

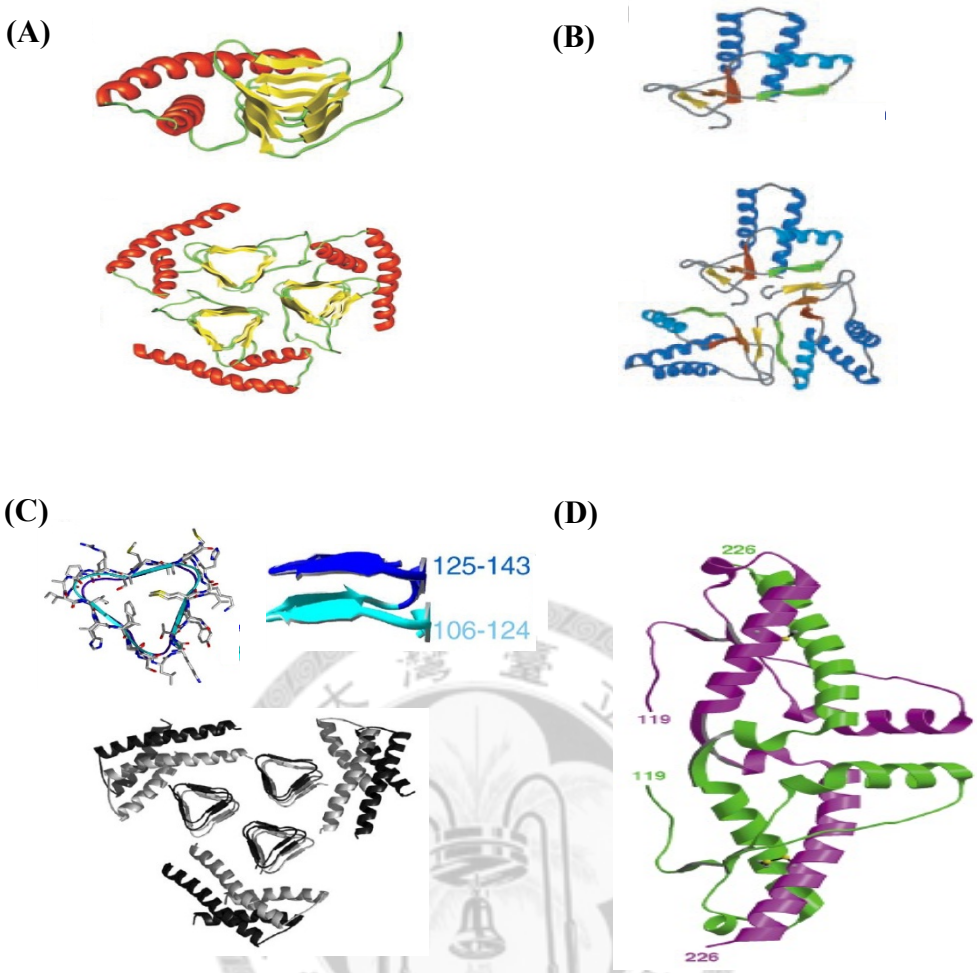

Figure 1.4 Different models of PrP^{Sc}. (A) The β-helical model. Residue 89-175 is in left-handed β-helix conformation, while the α-helices 2 and 3 are largely preserved as in the native structure. The β-helical domains of PrP associate into trimers. (Govaerts et al, 2004) (B) The β-spiral model. Two native β-strands and two newly formed β-strands comprise the amyloid core, while three α-helices retained. (DeMarco & Daggett, 2004) (C) The two-rung model. Two β-helix rungs are composed of residue 125-143 and residue 106-124, respectively. Amyloid core is left-handed β-helix trimers and C-terminal α-helices are retained. (Langedijk et al, 2006) (D) The domain-swapping model. The dimer came from the three-dimensional swapping of the C-terminal helix 3 and rearrangement of the disulfide bond

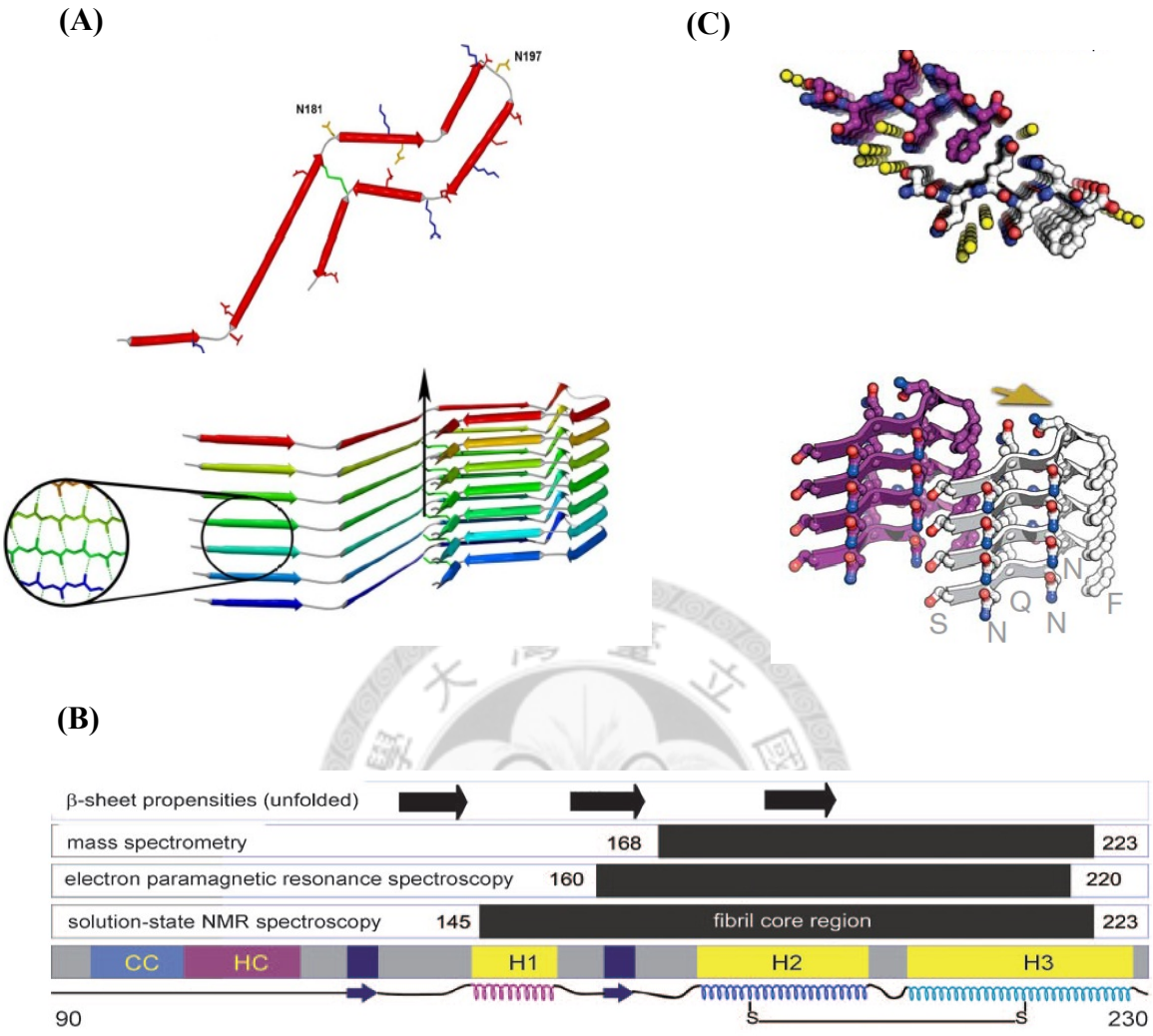

Figure 1.5 Different PrP^{Sc} models from experimentally results. (A) The parallel, in-register β-structure model. Human rPrP90–231 fibrils revealed residues 160–220 are the amyloid core region. Monomers stacked to form single-molecule layers so that same residues could be perfectly aligned by the long fibrillar axis (arrow). (Cobb et al, 2007) (B) Schematic presentation of fibril core of recombinant prion hPrP90–230 amyloid fibrils as investigated by different techniques. The observed β-sheet propensities are shown by black arrows. The charged cluster (CC), hydrophobic core (HC), helices (H1, H2 and H3) and single disulfide bridge from native structure are indicated. (Kumar et al, 2010) (C) The steric zippers model. Amyloid-like fibrils formed by prion peptide show steric zippers structure. (Sawaya et al, 2007)

1.6 Electron spin resonance (ESR)

Structural analysis of protein folds is most often performed using Nuclear Magnetic Resonance (NMR) spectroscopy or X-ray crystallography. However, large molecular weight proteins and proteins that are highly dynamic in solution or uneasily crystalized proteins are not always amenable to these high resolution techniques. Furthermore, structures obtained by crystallography do not always represent the biologically active conformation of the protein in solution (Cooke & Brown, 2011). Electron spin resonance (ESR), or called electron paramagnetic resonance (EPR), combines with site-directed spin labeling (SDSL) as pioneered by W. L. Hubbel and co-workers offers a powerful method for the studying structure and dynamics of protein (Hubbell & Altenbach, 1994).

This technique introduces a cysteine residue into the protein backbone and then it is covalently attached with sulfydryl specific nitroxide spin label by formation of a disulfide bond. Nitroxides are stable free radicals and contain an unpaired electron required for ESR detection which is localized on the N–O bond. According to quantum theory, the electron has a spin which can be understood as an angular momentum leading to a magnetic moment. As the spins of the electrons paired on molecular are compensated because of Pauli's principle of exclusion, only unpaired

electrons take part in the resonance phenomenon. Since many biological macromolecules are diamagnetic, the nitroxide resonance on the specific cysteine allows targeted analysis of protein structure. In the present of an external magnetic field, the electron's spin splits into two different energy states, parallel orientations ($m_s = -\frac{1}{2}$) (m_s: the spin magnetic quantum number) or antiparallel ($m_s = +\frac{1}{2}$) relative to this field (fig. 1.6). This phenomenon is called Zeeman effect. ESR spectroscopy is the technique for detection of the specific (resonant) absorption of energy (usually microwave radiation), which matches the distance between the Zeeman levels. The general principle can be described by the following formula:

$$\Delta E = h\nu = g\beta H \qquad \text{(eq. 1)}$$

where ΔE is the energy of resonant absorption, h is Planck's constant, ν is microwave frequency, β is Bohr magneton, a constant related to electron charge and mass, H is magnetic field at which resonance occurs, and g is a spectroscopic factor (tensor) which is a characteristic of a given paramagnetic center. The g factor can provide important information on the electron density distribution and geometry of the paramagnetic system. The general ESR spectrum comes from the absorption curve after the 1st derivation (fig. 1.6). Since the source of an ESR spectrum is a change in an electron's spin state, it might be thought that all ESR spectra for a single electron spin would consist of one line. However, the interaction of an unpaired electron with nearby

nuclear spins results in additional allowed energy states and multi-lined spectra. This is called hyperfine interaction. For instance, the electron spin of MTSSL interacts with nearby nitrogen and splits the ESR signal into three lines.

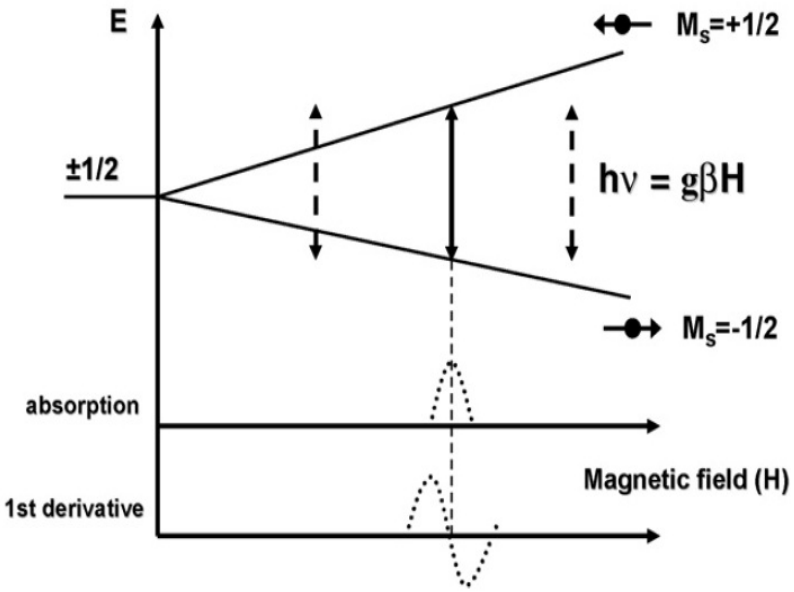

Figure 1.6 The general principle of electron spin resonance (ESR) spectroscopy. The external magnetic field (*H*) interacts with electron magnetic moments resulting in appearance of the energy difference between spin states and dividing electrons into two groups (either parallel or anti-parallel to *H*). When the energy difference between the spin states of paramagnetic system becomes equal to the microwave energy (*hν*), the absorption occurs. The details of spectral line bear important information on the interactions of unpaired electrons; therefore, in order to allow phase sensitive detection, the magnetic field is modulated (with modulation coils) resulting in the derivative spectrum outcome. (Kleschyov et al, 2007)

The following information can be obtained from SDSL-ESR experiments: (1) side chain mobility, (2) distances to other spin label, (3) solvent accessibility, and (4) the environment of the spin-label. The important ESR parameters are the shape and the

width of the spectral line, which are depended on spin mobility and inter-spin distance. The mobility of a spin label is due to the movement of the entire protein and to an ensemble of different local movements including local backbone fluctuations and internal dynamics of the spin-labeled side chain. When the spin labels are able to tumble rapidly in an isotropic way, magnetic interactions are completely averaged and the ESR spectrum displays three narrow lines. As the motions are slower, the magnetic anisotropy is no longer totally averaged, so the ESR signals become broader (Longhi et al, 2011) (fig. 1.7). Furthermore, distance measurements by ESR are relied on the dipole–dipole interactions between spins. The distance measurements which can be observed by continuous wave (CW) ESR spectroscopy are in the range of 8-25 Å. This distance range can be further extended up to approximately 80 Å using pulsed ESR methods.

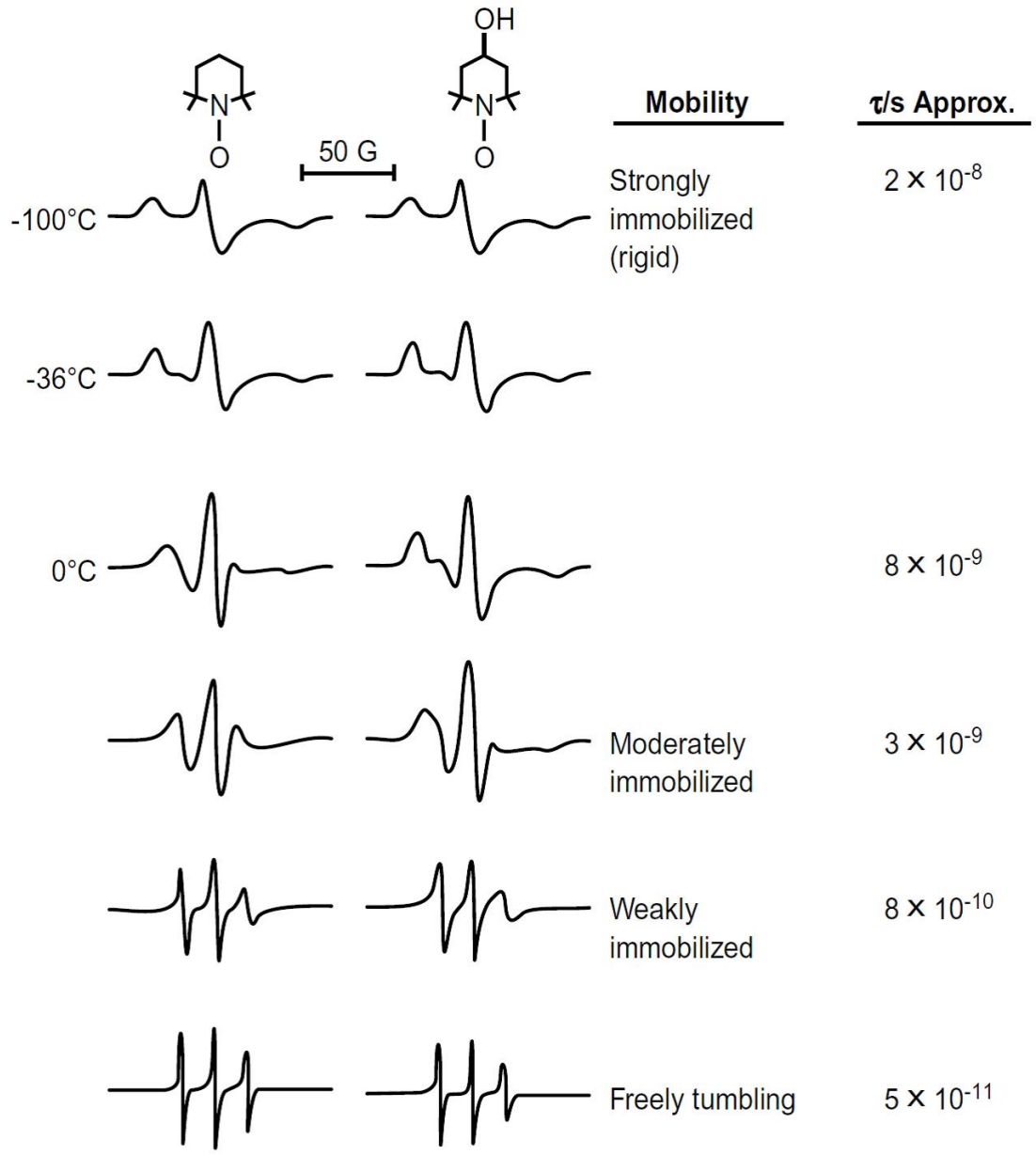

Figure 1.7 ESR spectra of spin labels for nitroxides under various conditions of rotational mobility. The effect of viscosity on the line shapes and rotational correlation times τ is shown. (Hammes, 2005)

1.7 Previous study in our lab

In our previous study, we found that disulfide bond was important for PrP structural stability. When dissolved in native condition (10 mM NaOAc, pH 7), $mPrP^{wt}$ was mainly α-helix structure, but disulfide bond removed PrP showed predominant β-structure by circular dichroism spectroscopy (CD). Interestingly, analytic ultracentrifugation (AUC) and transmission electronic microscopy (TEM) suggested that this kind of β-PrP were oligomers. Furthermore, β-PrP was sensitive to proteinase K and showed high ThT fluorescence. Compare to previous reports which prion oligomers were generated from denaturing or acidic conditions (Baskakov et al, 2002; Jackson et al, 1999), our β-PrP oligomers were produced under native condition. Moreover, the structural transition process can be monitored by CD under lower salt condition (0.5 mM NaOAc, pH 7). The disulfide bond-deletion PrP was spontaneously converted from α-helix structure to β-sheet predominant structure. In addition, we used SDSL-ESR technique and found that residue 132 is still flexible when mutant PrP becomes β-oligomers. Helix 2 may be partially unfolded in β-structure. Overall, disulfide bond-deletion PrP is a useful model for studying structure conversion of prion protein under the native condition.

1.8 The aim of the thesis

Until now, we have limited understanding about prion disease because the PrP^{Sc} structure and prion misfolding mechanism are still unclear. Since high resolution structure of PrP^{Sc} is hard to get from NMR or X-ray diffraction, we have to use indirect approach to study prion structure. As seen in section 1.5, plenty of PrP^{Sc} models have been proposed, but none one of them could be widely accepted.

In this thesis, we attempted to investigate the structural conversion mechanism of prion protein and which part of the protein was involved in this transition. Based on the model which was established by our previous study, further details about structural transition were achieved. We first designed more mutant position on prion protein including all three α-helices for the purpose of getting more information from different regions. Then we transformed mutant PrP into different structures, including β-oligomers, spontaneous structural conversion and amyloid fibrils. The experiments were combined with CD, TEM, SDSL-ESR techniques and so on. According to the ESR spectra from different regions or different structures, we can explore the role of three α-helices during the structural change.

Chapter 2 Materials and Methods

2.1 Materials

2.1.1 Water

Water was distilled and deionized by Milli-RO PLUS 60 and Milli-QSP reagent water system.

2.1.2 Chemicals

Chemicals	Sources
40% acrylamide/bis (29:1) solution	Bio-Rad
Absolute ethanol	Riedel-de Haën
Antiform 204	Sigma
Acetic acid	Sigma
Acetic acid, glacial	J.T. Baker
Acetonitrile	J.T. Baker
Agar (Bacteriological grade)	Amresco
Agarose I (Biotechnology grade)	Amresco
APS (ammonium persulfate)	Amresco
Ampicillin, sodium salt	Amresco
Bis-Tris	Sigma

Bromophenol blue	Amresco
CelLytic B 10X reagent	Sigma
Coomassie brilliant blue R-250	Sigma
DMSO (dimethyl sulfoxide)	Amresco
DNaseI	Roche
DpnI restriction enzyme	Roche
EDTA (ethylenediaminetetraacetic acid)	J.T. Baker
ethanol	J.T. Baker
Glutathione, reduced	Sigma
Glutathione, oxidized	Sigma
Glycerol	Amresco
Glycine	Amresco
Guanidine hydrochloride	Bionovas
Hydrochloric acid 37 %	Riedel-de Haën
IPTG (isopropyl β-D-1-thiogalactopyranoside)	Amresco
LB medium	Aurora Biotech
Magnesium chloride	Sigma
MES [2-(N-morpholino)ethanesulfonic acid]	Sigma
Methanol alchohol, ahhydrous	Mallinckrodt

MTSSL	Enzo
Pepsin	Sigma
Potassium chloride	J.T. Baker
Peptone from caesin	Merck
PfuUltra high-fidelity DNA polymerase	Stratagene
PMSF (phenylmethanesulfonylfluoride)	Sigma
Silica, mesostructured	Sigma
SDS (sodium dodecyl sulfate)	Amresco
Sodium acetate	Sigma
Sodium chloride	Sigma
Sodium hydroxide	Sigma
Sodium phosphate monobasic	Sigma
Sodium phosphate dibasic	Sigma
T4 DNA ligase	Roche
TAE buffer (50X)	Amresco
TCEP (*tris*(2-carboxyethyl)phosphine)	Sigma
TEMED (N,N,N',N'-tetramethylethylenediamine)	Amresco
TFA (trifluoroacetic acid) 99 %	Acros
ThT (thioflavin T)	Sigma

Tris	Amresco
Tris hydrochloride	J.T. Baker
Urea	Amresco
Yeast extract	Merck

2.2 Methods

2.2.1 Expression construct and site-directed mutagenesis

Mutant prion protein constructs, including mPrP-CtoA, S132C, N181C and S132C/N181C, were the previous work made by our lab. Two other new constructs, D147C and Q217C, were generated from mPrP-CtoA plasmid by PCR-based strategy. In the strategy, forward primers were designed according to the desired mutant; then 5'-phosphorylation was added to the forward primers for ligation. Reversed primers were same as the original sequences. Wild-type mPrP ($mPrP^{wt}$) in pET101/D-TOPO vector was derived from Ilia V. Baskakov (University of Maryland Biotechnology Institute, USA). Primer sequences for the mutations were listed below: (mutation sites were underlined.)

D147C forward: 5'-TGCCGCTACTACCGTGAAAACATG-3'

D147C reversed: 5'-CTCCCAGTCGTTGCCAAAATGGAT-3'

Q217C forward: 5'-TGCTACCAGAAGGAGTCCCAGGCC-3'

Q217C reversed: 5’-GGTGACGGCCATCTGCTCCACCAC-3’

PCR-amplified products were treated with DpnI to digest parental plasmids. DNA purification was done by QIAquick Nucleotide Removal Kit (QIAGEN, USA) and ligation was done by Rapid DNA Ligation Kit (Roche, USA). Then ligated plasmids were transformed into DH5α™ competent cells (Invitrogen, USA) and purified with QIAprep Spin Miniprep Kit (QIAGEN, USA). The positive clones were selected and checked by ABI 3730 Sequencer. Vector NTI (version 9.1.0, Invitrogen) program and its component, AlignX, were used to align DNA sequences and to generate mPrP construct maps.

2.2.2 Small-scale protein expression

Transformed BL21 Star™ (DE3) competent cells (Invitrogen,USA) were inoculated into LB medium with 100 μg/ml ampicillin and incubated overnight at 37 ℃, 250 rpm. About 0.5 mL overnight culture was subcultured into 4.5 mL LB/ampicillin medium and incubated at 37 ℃, 250 rpm for 1 hr. In order to induce protein expression, 1mM IPTG was added into cell culture and it was incubated for 8 hr at 37 ℃, 250 rpm. Then the cell culture was centrifuged at 16,000 g for 1 min and the supernatant was removed. The pellet was resuspened by 300 μL lysis buffer (50 mM

Tris-HCl, 100 mM NaCl. pH 8.0). Cell lysis was done by adding 0.5 X CelLytic B, 0.15 mg/mL lysozyme, 25 μg/mL DNaseI, 7 mM $MgCl_2$, and 1 mM PMSF. Then the expression efficiency was checked by SDS-PAGE electrophoresis.

2.2.3 Large-scale protein expression, purification, and identification

2.2.3.1 Glycerol cell stock preparation

Transformed competent cells were prepared as glycerol stock for the purpose of a stable quality of expression yield and convenience of storage. About 0.5 mL overnight cell culture was added into 3.5 mL LB/ampicillin medium and was incubated for 3 hr at 37 ℃, 250 rpm. Then cell culture was mixed with 0.8 mL sterile glycerol and kept at -20 ℃ overnight. Cell culture was finally stored at -80 ℃ for long term storage. Typically, 200 μL glycerol stocks were used for 1.2 L culture protein expression.

2.2.3.2 Expression of recombinant mouse PrP in *E. coli* and cell lysis

For 2.4-liter culture expression (each 600 mL medium in a 2-liter flask), 400 uL cell stocks were added to 48 mL LB/ampicillin medium and were incubated overnight at 37 ℃, 250 rpm. Then cell culture was subcultured into 2.4 L fresh TB/ampicillin medium and was incubated for 3 hr at same condition. Protein expression was induced by 1 mM IPTG at 37 ℃ for 5 hr. Cell pellet was collected by centrifuging at 1,900 g

for 10 min at 4 ℃. Typically, we can get about 20 g cell pellets from 2.4 L cultured medium. The cell pellet was resuspended by lysis buffer (50 mM Tris, 100 mM NaCl, pH 8.0), and cell lysis was done by adding 0.5 X CelLyticB, 0.15 mg/mL lysozyme, 25 μg/mL DNaseI, 7 mM $MgCl_2$, and 1 mM PMSF. The final volume of cell lysate should be 8.7 mL per gram of cell pellet. Then the cell lysate was stirred for 30 min at room temperature and centrifuged at 6,000 g for 30 min at 4 ℃. Because recombinant prion protein was existed in the inclusion body, we discarded the supernatant and keep the pellet at -30 ℃.

2.2.3.3 Immobilized metal-ion affinity chromatography (IMAC)

The cell pellet was resolved by fresh IMAC A buffer (8 M urea, 100 mM Na_2HPO_4, 10 mM Tris-HCl, 1 mM TCEP, pH 8.0) with rotating for 2 hr at room temperature. Supernatant was collected by centrifuging at 18,000 g for 20 min at 4 ℃ and then was applied to the pre-packed column with Ni^{2+}-charged Chelating Sepharose Fast Flow (GE healthcare, USA). In order to enhance the specific binding, column was shaking for 30 min at 4 ℃. After that, the column was washed with 5 column value (CV) IMAC A buffer for removing the non-specific binding materials. The target protein was eluted by 5 CV IMAC A buffer supplemented with 20 mM EDTA. For $mPrP^{wt}$ purification, TCEP was replaced by 10 mM reduced glutathione as the reducing agent.

2.2.3.4 Desalting and disulfide bond formation for $mPrP^{wt}$

$mPrP^{wt}$ was desalted to remove the reducing agent before oxidation to form disulfide bond. For the desalting step, XK-16 column, pre-packed with Sephadex G-25 Superfine (GE Healthcare, USA), was used on ÄKTAprime™ plus FPLC system (Amersham Biosciences, USA). Desalting buffer (6 M urea, 0.1 M Tris-HCl, pH 7.5) and the samples should be filtered by 0.45 μm Millipore syringe filter. About 10 mL sample was injected into pre-equilibrated column with the flow rate at 2 mL/min. Proteins were eluted about 10 mL (retention volume) prior to the elution of small molecules. Disulfide bond formation was done by incubating protein overnight at RT with 5 mM EDTA and 0.2 mM oxidized glutathione.

2.2.3.5 HPLC purification and protein identification

IMAC eluent, which was for mutant mPrP, or oxidized sample, which was for $mPrP^{wt}$, was directly applied to reversed-phase C5 column (Discovery BIO Wide Pore C5, 10 μm, 25 cm x 10.0 mm, Supelco, USA) with Jasco (Japan) or Agilent (USA) HPLC system. Buffer A (94.9 % water, 5 % acetonitrile, 0.1 % TFA), Buffer B (99.9 % acetonitrile, 0.1 % TFA) and protein sample were filtered by 0.45 μm Millipore syringe filter before purification. The purification condition was as below: The B buffer concentration was raised from 29 to 47 % in gradient within 30 min at the flow

rate of 3 mL/min. Mutant mPrP was typically eluted at 31-33 %. About 10 mg mutant proteins were accessible after the HPLC purification from 2.4 L TB/ampicillm medium. Protein can be long-term preserved as powder at -30 ℃ after lyophilized (MAXI dry lyo, Heto, Denmark).

Protein purity and identification can be examined by SDS-PAGE or mass spectrometry (MS). For SDS-PAGE, protein sample was mixed with sample buffer (50 mM Tris-HCl pH 6.8, 2% SDS, 10% glycerol, 1% β-mercaptoethanol, 12.5 mM EDTA, 0.02 % bromophenol blue) and was heated at 100 ℃ for 10 min. Electrophoresis was performed in 12 % SDS-PAGE under 120 V for 120 min. The gel was stained by coomassie brilliant R-250 solution. Then destained by water/methanol/acetic acid mixture (6:3:1). For ESI-TOF MS, QSTAR XL system (Applied Biosystems) or Q-TOF Ultima API Mass Spectrometer (Macromass) was used and combined with nanospray method.

Protein concentration can be measured by Beckman DU 800 UV-Visible spectrophotometer (Beckman Coulter, Inc., USA) or ND-1000 Spectrophotometer (NanoDrop Technologies Inc., USA) at UV 280 nm absorption. Molar extinction coefficient (ε) for $mPrP^{wt}$ and mutants was 80143.

2.2.4 Secondary structure analysis by circular dichroism and CDPro

Far-UV Circular dichroism (CD) is a powerful technique to study protein secondary structure. For CD experiment, sample concentration was above 0.1 mg/mL and 0.1 cm path-length quartz cuvette (HELLMA) was used. CD signal was measured by Jasco J-715 spectropolarimeter at the wavelength from 195 nm to 250 nm with a band width of 2.0 nm. Scan speed was 20 nm/min and response time was set to 0.125 sec. CD signal was performed as mean residue ellipticity (MRE) and further smoothed by OriginPro 8 SR1.

CDPro software package consisted of three popular programs, (SELCON3, CDSSTR, and CONTIN), they were used for analyzing the protein CD spectra for determining the secondary structure fractions. Another program, CLUSTER, was used for determining tertiary structure class. For secondary structure analysis, the unit of CD signal data was transformed into Δε by CRDATA program and deconvoluted by CDSSTR algorithms. Reference set SP43 was used in the fitting. NRMSD values were better less than 1.00.

2.2.5 Analytical ultracentrifugation (AUC)

Sedimentation velocity analytical ultracentrifugation (SV-AUC) experiment was

carried out by using Beckman Coulter Analytical Ultracentrifugation XL-A. Sample was loaded into Beckman AUC sample cells with 12-mm optical path two-channel centerpieces, with the matched buffer in the reference sector. And then cells were loaded into a AnTi-60 rotor and spun at 60,000 rpm. Scans were acquired using absorbance at 280 nm at 10-min intervals over a period of 5-6 hr. Partial specific volume ($\bar{\nu}$), buffer density, and viscosity were calculated from the amino acid sequence by SEDNTERP software (version 1.09). For D147C and Q217C, the partial specific volume was 0.7095 and 0.7091. The buffer density and viscosity for 10 mM NaOAc were 0.99883 and 0.010043. The sedimentation profiles were analyzed and fit by SEDFIT (version 12.1b).

2.2.6 Fibril formation and ThT (thioflavin T) binding assay

In order to generate amyloid fibrils, protein was dissolved in 6 M GdnHCl with the concentration at 130 μM. Then protein/GdnHCl solution, water, and fiber formation buffer (6 M urea, 2 X PBS) were mixed by the ratio of 1:2:3, resulting in the final protein concentration at 22 μM. 1 X PBS (phosphate buffered saline) composes of 10 mM phosphate buffer (pH 7.4), 137 mM NaCl and 2.7 mM KCl. After that, the sample was incubated in 37 ℃ incubator with 250 rpm shaking for several days until fibrils forming. ThT (thioflavin T) binding assay was used to detect the process of

fibril formation. ThT is a benzothiazole dye which nonspecifically binds β-sheet structures. Fluorescence emission will dramatically increase to around 490 nm when the wavelength was excited at 420 nm after ThT binding.

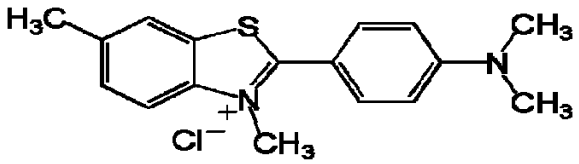

Figure 2.1 Structure of Thioflavine T (ThT).

ThT was prepared as 2 mM stock in ThT dilution buffer (140 mM KCl, 100 mM sodium phosphate buffer, pH 7.5). Working solution was freshly prepared before used by adjusting the final concentration to 200 μM. 30 μl aliquots of each sample were withdrawn at different time points and mixed with equal volume of 200 μM ThT solution. Fluorescence measurement was carried out by Jasco FP-750 spectrophotometer using a 3-mm path-length rectangular cuvette. The excitation wavelength was set to 420 nm. The fluorescence spectrum was recorded between 450 and 600 nm. The excitation and emission slits were set to 10 nm and 5 nm, respectively. The scanning speed of 125 nm / min with a data pitch of 1 nm was employed.

2.2.7 Transition electron microscopy (TEM)

A drop (15 μL) of sample was loaded on a carbon-only coated 300-mesh copper

grid and left for adsorption for 3 min. Then it was washed with 100 μL DI water and negatively stained with freshly filtered 2 % uranyl acetate for 3 min. After washed with 50 μL DI water, the grid was dried overnight. For oligomer sample, all the washing steps were escaped. The sample was viewed by Hitachi H7000 electron microscope operated at 75 kV.

2.2.8 Spin-labeling & purification

For ESR experiments, mutant proteins were labeled with (1-oxyl-2,2,5,5-tetramethylpyrroline-3-methyl) methanethiosulfonate spin label, abbreviated as MTSSL (Alexis biochemicals, San Diego, CA). The experiment procedure was shown as follows: First, 2 mg mutant protein was dissolved in 477 μL DMSO. Then 500 μL 50 Mm Tris (pH 7.5) and 20 μL TCEP (in DMSO) were added; typically this process would perform on ice because DSMO, which was mixed with water, would generate heat. This was followed by the addition of 2.7 μL MTSSL and overnight incubation with shaking at RT in the dark. (MTTSL compound should always be sheltered from light.) The molar ratio of per cysteine residue to MTSSL was 1:10. To remove free radicals and unlabeled protein, the spin-labeled protein solution was purified by reversed-phase HPLC. The methods for HPLC purification and protein identification were the same as above whereas the gradient used in HPLC was set to

29-41 %B in 40 min.

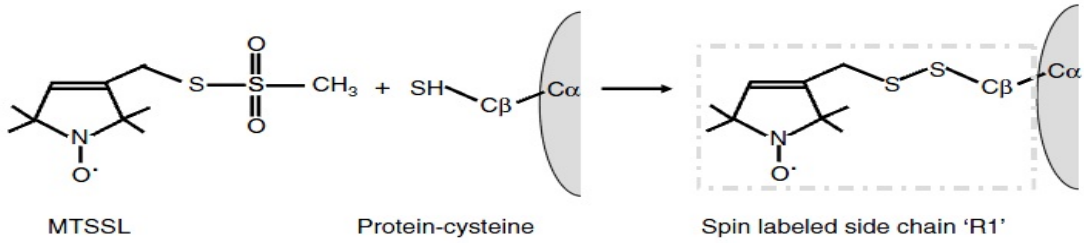

Figure 2.2 Spin labeling. MTSSL reacts with thiol groups of cysteine and then produces the nitroxide side chain designated R1. (Cooke & Brown, 2011)

2.2.9 Electron spin resonance (ESR)

The pre-treatment of ESR experiments for variant samples were different. For β-oligomers, protein samples were dissolved in 10 mM NaOAc firstly and concentration was about 0.45 mM. Then 20 μL protein samples were mixed with 20 μL 80 % sucrose. For spontaneous structural conversion experiments, protein samples were dissolved in 0.5 mM NaOAc and the concentration was also 0.45 mM. But 20 μL protein samples were added in 12 mg nanopore materials (Silica, mesostructured, Sigma). For fibril samples, the supernatant was removed after centrifugation; then 20 μL DI water was added to resuspend the fibrils, and the samples were mixed with 20 μL 80 % glycerol. In ESR measurements, liquid samples were loaded into two 0.8 mm (O.D.) capillaries; each was about 20 μl, and the ends of capillaries were sealed with parafilm. Two capillaries totally contained 40 μL samples were introduced into a 4 mm (O.D.) quartz ESR tubes which also sealed with parafilm. For nanopores and

fibril samples, they were directly loaded into 4 mm (O.D.) quartz ESR tubes. ESR spectra were measured by Bruker ELEXSYS E580 CW/Pulse spectrometer. The CW-ESR experiment was performed at an operating frequency of 9.4 GHz and 1.5 mW incident microwave power. The swept magnetic range was 200 Gauss. For different temperature scans, the spectrometer was equipped with an ER 4131VT variable temperature accessory.

2.2.10 Pepsin digestion assay

To investigate the amyloid core of fibril, pepsin was selected to digest fibril samples. Experimental procedure was modified from a previous report (Frare et al, 2006). The spin-labeled fibril samples were first measured by ESR to get spectra of undigested fibrils. And then directly added following materials into ESR tubes. Pepsin (sigma) was added at an E : S ratio of 1:15 (w/w). Additional 10 μL 80% glycerol can maintain the viscosity. According to pepsin property, about 5.4 μL 100 mL HCl was necessary for providing acid condition. The digested reaction must carry out for more than 30 min at room temperature. Finally ESR was used to measure the spectra of digested fibrils.

Chapter 3 Results (I)

3.1 Design and expression of mutant mouse prion protein constructs

To investigate the prion protein, we used full-length mouse prion protein (mPrP 23-231) as a model and constructed variant mutant. The $mPrP^{wt}$ construct was derived from Ilia V. Baskakov's group, University of Maryland, U.S.A. In our lab's previous work, we have made several mutants including mPrP-CtoA, S132C, N181C and S132C/N181C. mPrP-CtoA was a mutant which mutated all cysteine to alanine, so the disulfide bond was removed. Based on this disulfide-deleted variant, S132 (in the loop between Strand 1 and Helix 1) and N181 (in Helix 2) were individually or doubly mutated to cysteine, generating S132C, N181C, and S132C/N181C. Moreover, in order to study different domains, we selected another two mutation sites, D147 (Helix 1) and Q217 (Helix 3). On the purpose of spin labeling, we mutated the selected site to cysteine. D147C and Q217C were made by site-directed mutagenesis form mPrP-CtoA construct. All the mutant PrP sequences were carried by pET101/D-TOPO expression vector, which was shown in fig 3.1, and transformed into DH5α™ competent cells for proliferation. DNA sequences were confirmed by DNA sequencing. Figure 3.2 shows different mutation site of the mouse prion protein.

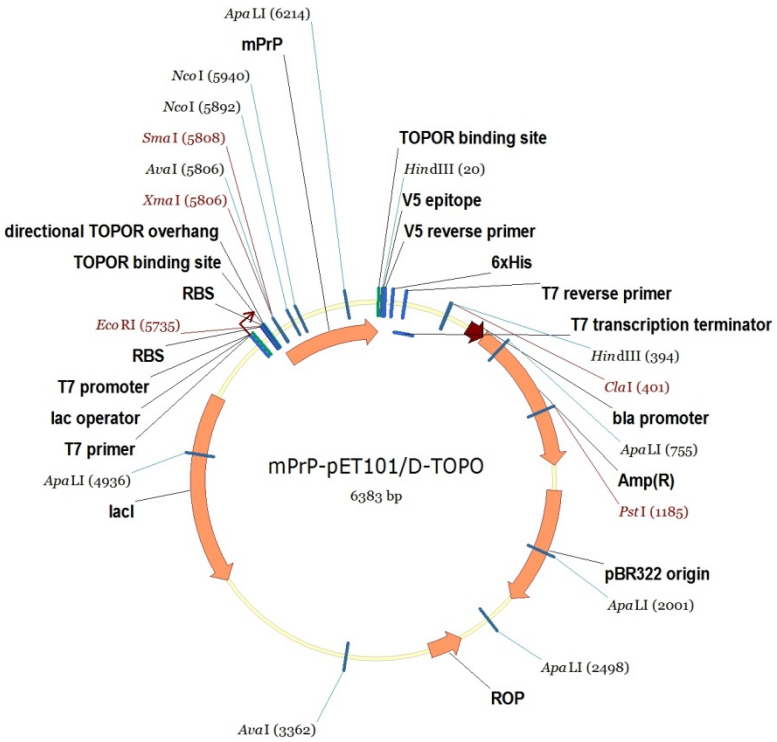

Figure 3.1 pET101/D-TOPO expression vector. The mPrP gene and variant mutants were inserted into pET101/D-TOPO expression vector.

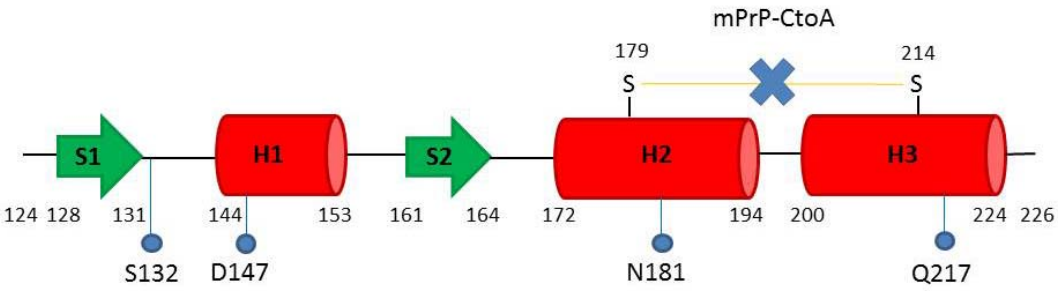

Figure 3.2 Different mutation site of mPrP. C179 and C214 were replaced by alanine to remove disulfide bond. Residue S132, D147, N181 and Q217 located on different regions and were substituted to cysteine (the residue number follows hamster PrP sequence).

3.2 Small-scale expression analysis

Expression pattern of mutant PrP was determined by small-scale expression test. Expression vectors with mutant PrP sequence were transformed into BL21 Star™ (DE3) competent cells. As shown in fig 3.3, D147C (MW=22987) expression level was obviously induced by adding 1mM IPTG. Furthermore, mutant protein was existed in pellet after cell lysis and centrifugation. This result suggested that recombinant prion protein was in inclusion body. Q217C and D147C showed similar expression pattern.

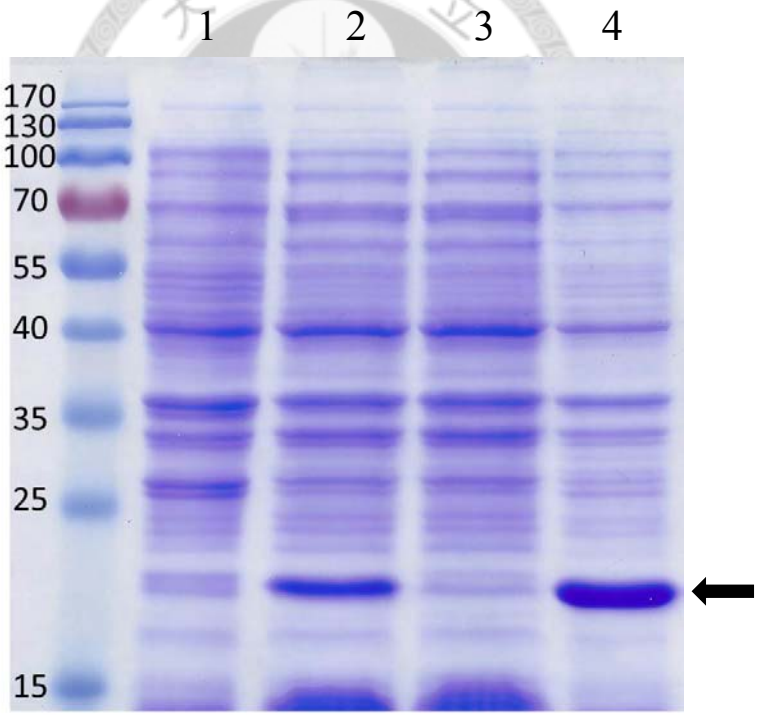

Figure 3.3 Small-scale expression of D147C. Lane 1: cell lysate from uninduced culture. Lane 2: cell lysate from 1 mM IPTG induced culture. Lane 3: supernatant of cell lysate after centrifugation. Lane 4: pellet of cell lysate after centrifugation. The black arrow indicates the PrP position.

3.3 large-scale expression

To get enough amount of mutant protein for experiments, we harvested transformed competent cell in large scale. *Escherichia coli* is a well-known model and is used to produce recombinant protein. However, the expression efficiency of prion protein was low and easily degraded. Therefore, we developed a fast, reliable method based on the protocol from Baskakov's group (Makarava & Baskakov, 2008) for expression and purification of wild-type and mutant PrP. At first, we prepared glycerol stock with transformed competent cells and stored it at -80 ℃, ensuring constant protein expression for every batch. For large-scale expression, overnight *E. coli* culture was cultured in 2.4 L TB medium and then induced protein expression by adding 1 mM IPTG. After cell lysis and centrifugation, we resolubilized cell pellet by IMAC A buffer which contained 8 M urea. Figure 3.4 shows the highly resolubilized efficiency of Q217C.

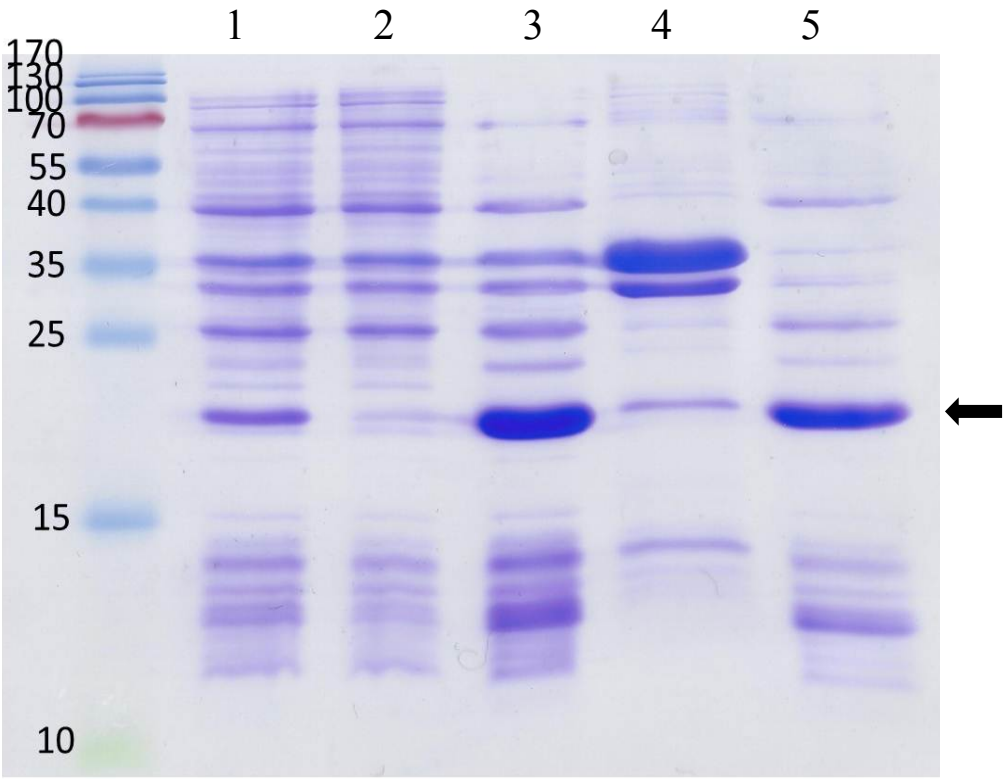

Figure 3.4 Resolubilization of Q217C from large-scaled expression culture. Lane 1: 1 mM IPTG induced cell lysate. Lane 2: supernatant of cell lysate after centrifugation. Lane 3: pellet of cell lysate after centrifugation. Lane 4: pellet of 8 M urea resolubilization. Lane 5: supernatant of 8 M urea resolubilization. Black arrow indicates the PrP position. Most of PrP can be resolubilized in 8 M urea.

3.4 Purification by immobilized metal-ion affinity chromatography (IMAC)

According to the characteristic of prion protein, metal-ion affinity chromatography (IMAC) was used as the first step of purification. IMAC is a practical method to purify target proteins which possess metal-ion binding ability. Sometimes targeted proteins need extra His-tag to amplify the binding affinity. But prion protein contains octapeptide repeat regions which can bind to metal-ion (M.P. Hornshaw, 1995). Here, Ni^{2+}-charged column was used to purify resolubilized PrP. Wash step was able to remove unbound proteins while PrP was retained. As shown in fig 3.5, PrP was eluted

out by 20 mM EDTA. However, the protein purity was not satisfied and further HPLC purification was applied.

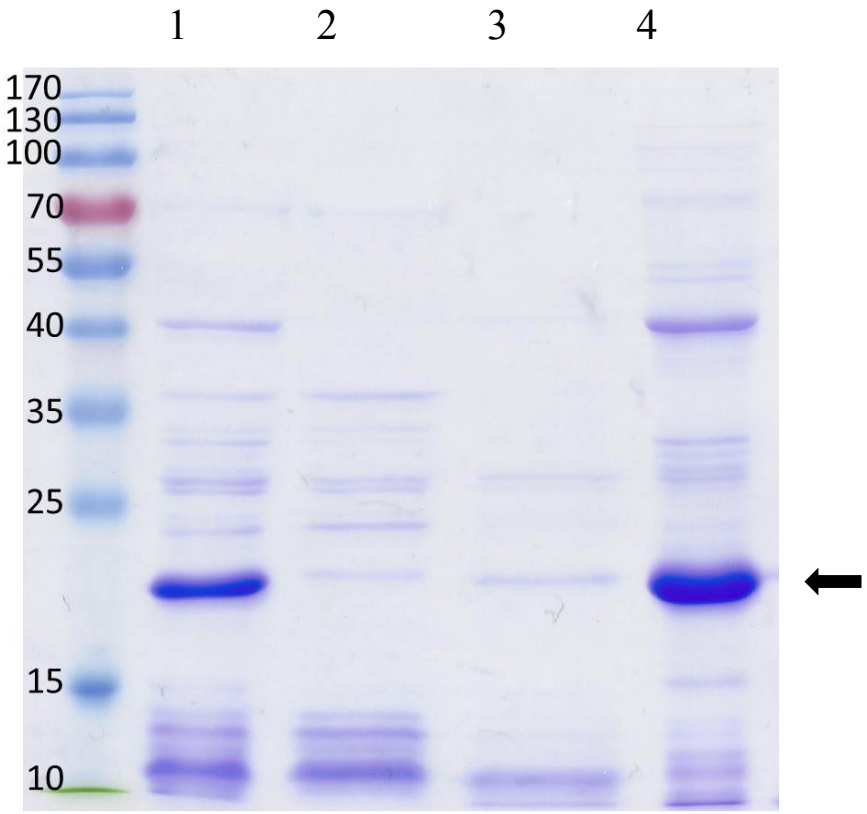

Figure 3.5 IMAC was used for Q217C purification. Lane 1: PrP samples before IMAC purification. Lane 2: Flow through fraction of IMAC. Lane 3: Wash fraction of IMAC. Lane 4: Elute fraction of IMAC. Black arrow indicates the PrP position.

3.5 Desalting and disulfide bond formation for mPrP^{wt}

For mPrP^{wt} purification, desalting and cysteine oxidation were additional steps after IMAC. Generally, native PrP^{C} contains one intramolecular disulfide bond in eukaryotic cell. Therefore, constituting the disulfide bond in recombinant wild type PrP was necessary. The desalting step was used to separate the protein from reduced

glutathione, ensuring that the following oxidation reaction was not affected by reduced glutathione. Desalting was completed by size-exclusion chromatography with FPLC system. Protein was eluted prior to salts and could be detected by UV absorption at 280 nm. After desalting step, disulfide bond formation was done by incubating protein overnight at RT with 5 mM EDTA and 0.2 mM oxidized glutathione.

3.6 High-performance liquid chromatography (HPLC) purification

High-performance liquid chromatography (HPLC) was the final step to purify $mPrP^{wt}$ and mutant variants. HPLC is a powerful technique for separating the individual components from mixtures. According to the hydrophobic interaction between PrP and alkyl group, reverse phase HPLC with C5 column was chosen to purify PrP. HPLC has high resolution and can clearly separate reduced form $mPrP^{wt}$ and oxidized form $mPrP^{wt}$. On the other hand, mutant PrP refolded itself into native structure by removing urea during HPLC. Typically, PrP was eluted at 33 % acetonitrile with slightly variant among different mutant PrP. Each mutant PrP showed single peak in HPLC chromatogram (fig. 3.6), suggesting that a high-purity protein was obtained.

(A)

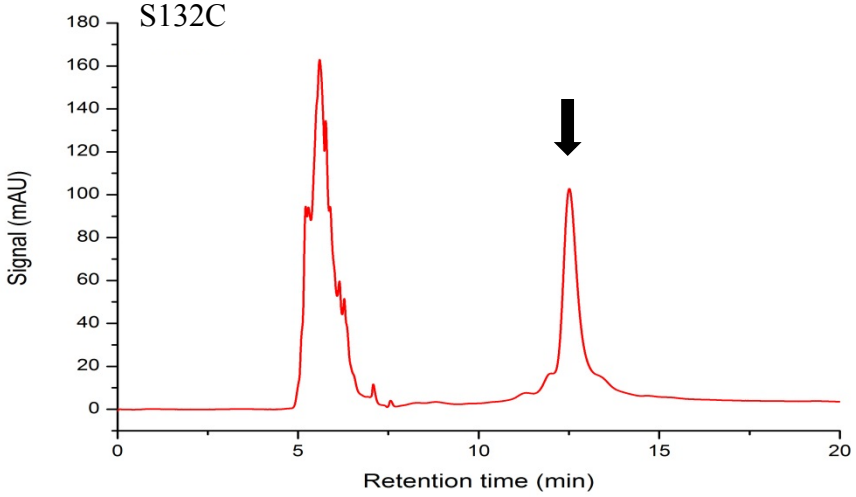
S132C
Signal (mAU)
Retention time (min)

(B)

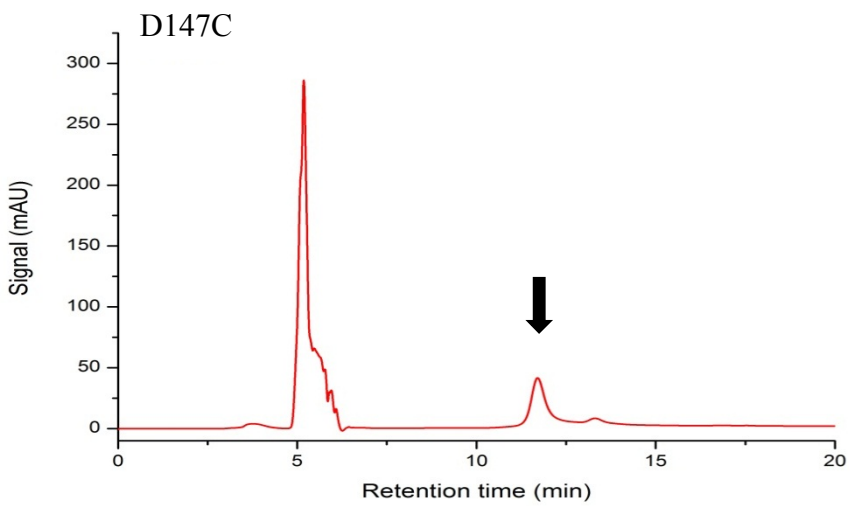
D147C
Signal (mAU)
Retention time (min)

(C)

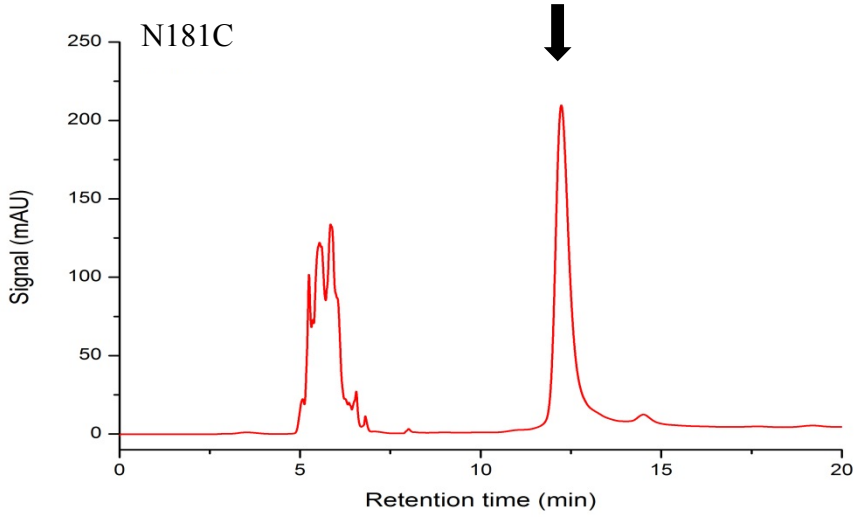
N181C
Signal (mAU)
Retention time (min)

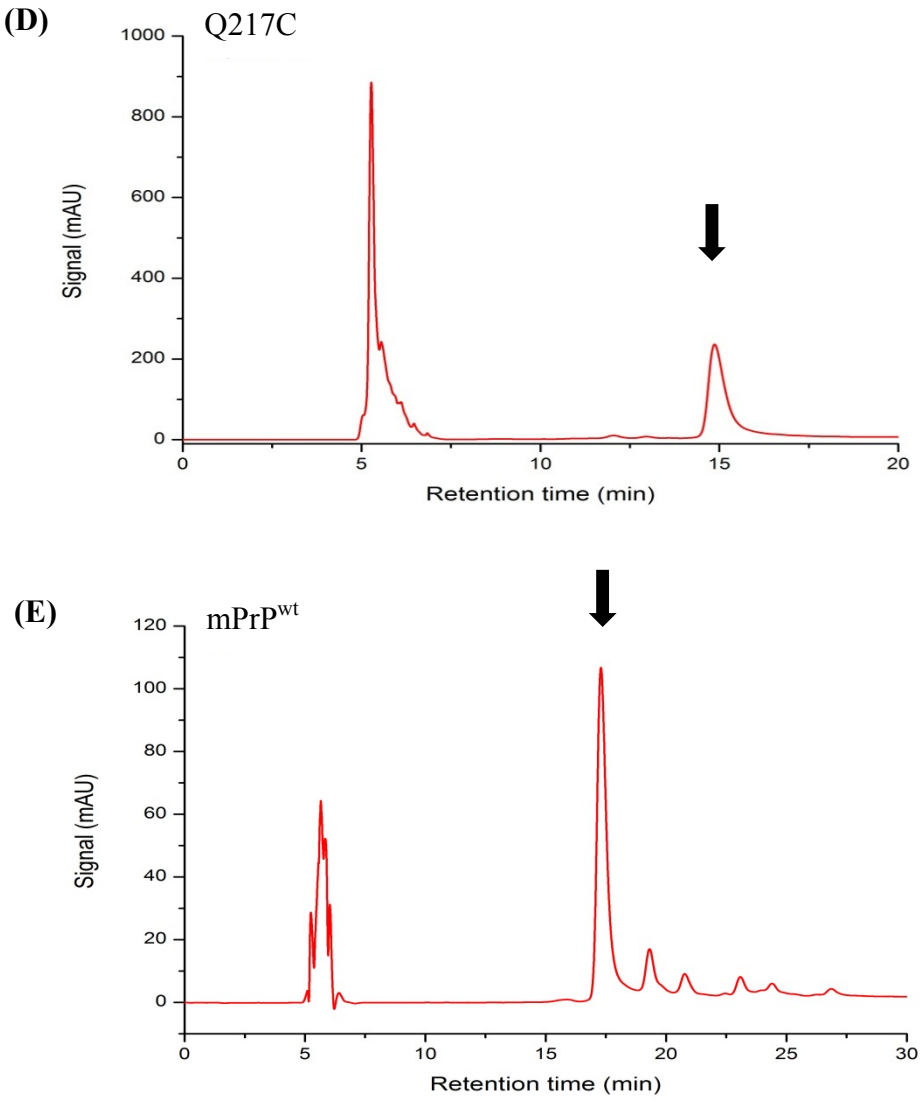

Figure 3.6 HPLC chromatograms of mPrP^{wt} and variant mutants. UV absorptions at 280 nm of HPLC purification are shown. The B buffer gradient for mPrP^{wt} was increased from 22 % to 40 % in 30 min. The B buffer for mutant prion proteins were increased from 29 % to 47 % in 30 min. The black arrow indicates the PrP position.

3.7 Spin-labeling and purification

Adding a spin label on mutant protein is essential for electron spin resonance (ESR) experiments. Mutant proteins were labeled with a 10-fold excess of a (1-oxy-2,2,5,5-tetramethyl-3-pyrroline-3-methyl) methanethiosulfonate spin label

(MTSSL) (Alexis Biochemicals, San Diego, CA) per cysteine residue overnight in the dark. The sulfydryl specific nitroxide spin label (MTSSL) can covalently attach via the formation of a disulfide bond with a cysteine residue of mutant protein. The ESR signals arise from the unpaired electron on the nitroxide group. The side chain with the MTSSL probe was designated as R1. After overnight spin-labeled reaction, HPLC was used to purify the spin labeled protein. To distinctly separate labeled proteins from unlabeled proteins, the buffer gradient was set from 29 % to 41 % buffer B within 40 min. The labeling yield was slightly different for different mutant proteins but at least 70 % proteins can be successfully labeled (fig. 3.7). All mutant proteins showed a very similar and high yield of labeling, indicating that the chosen labeling sites were highly accessible to solvent.

(A) S132R1

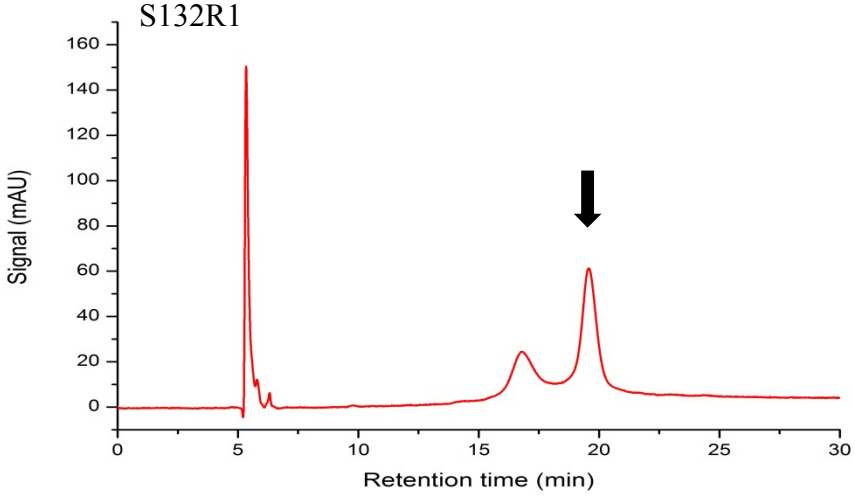

(B) D147R1

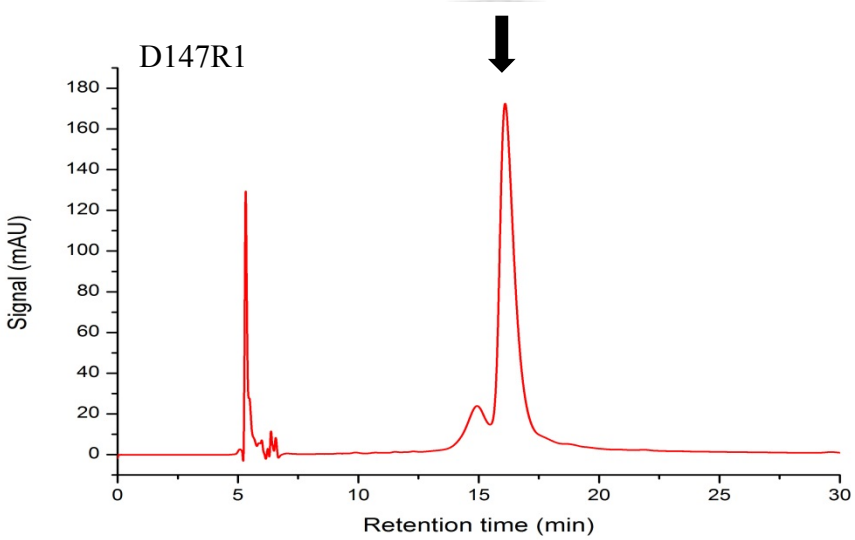

(C) N181R1

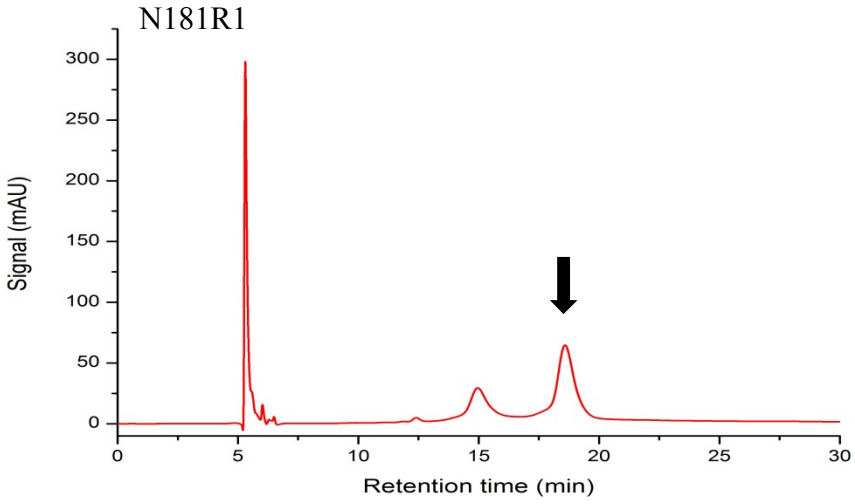

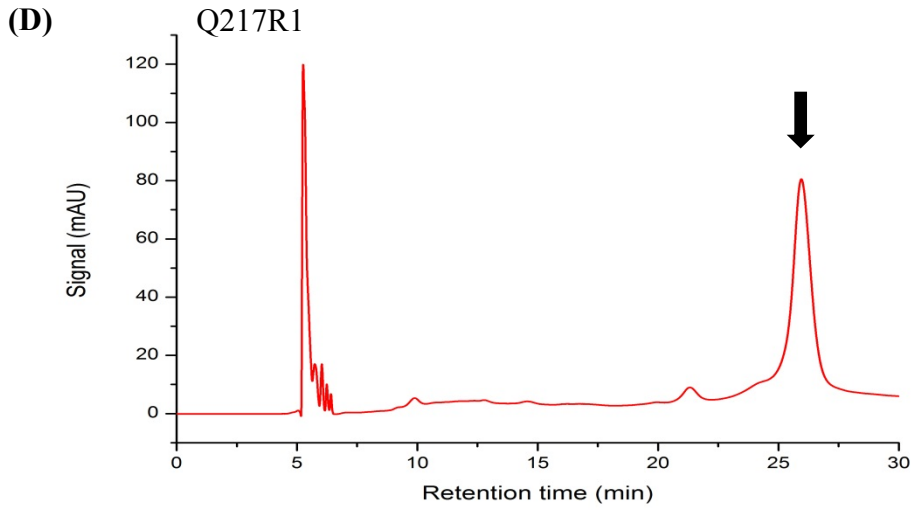

Figure 3.7 HPLC chromatograms of spin-labeled mutant proteins. UV absorptions at 280 nm of HPLC purification were shown. The B buffer percentage was increased from 29 % to 41 % in 40 min. The black arrow indicates the labeled protein position. The previous peak was unlabeled protein.

3.8 Protein identification and storage

To ensure the molecular weight and protein identification, each mutant protein and each spin-labeled protein was subjected to ESI-TOF MS after HPLC purification with the use of nanospray method. Figure 3.8 shows deconvolution results of ESI-MS spectra. After MTSSL-labeled, the PrP molecular weight would increase 184.3 Da. Only after the molecular weight was confirmed, then we started the following experiments. In 2.4 L cell culture, we could get about 10 mg of mutant proteins. All the purified mutant proteins were lyophilized and stored at -80 ℃.

(A)S132C

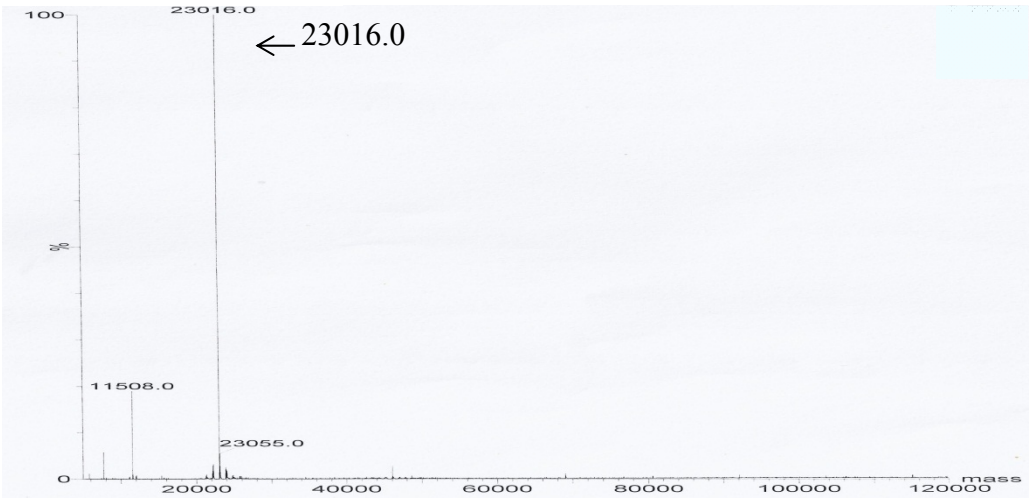

(B)D147C

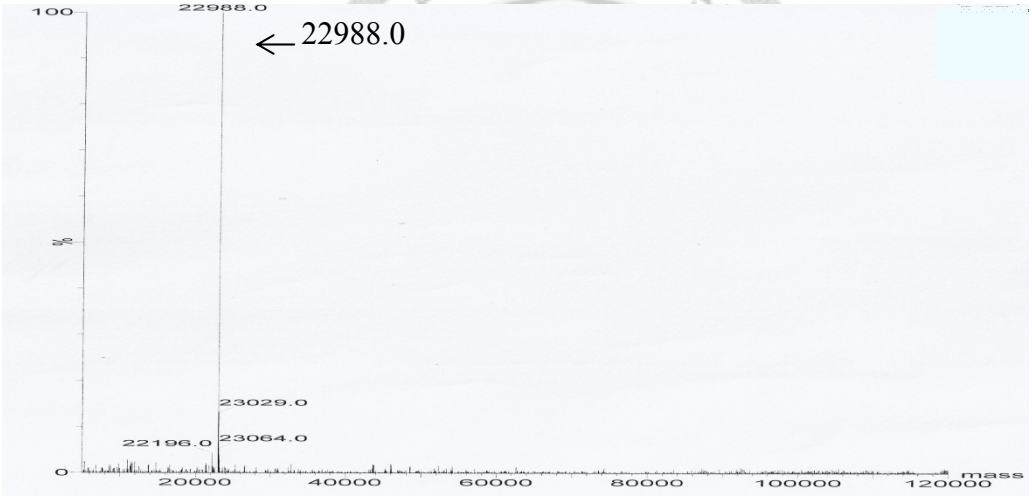

(C)N181C

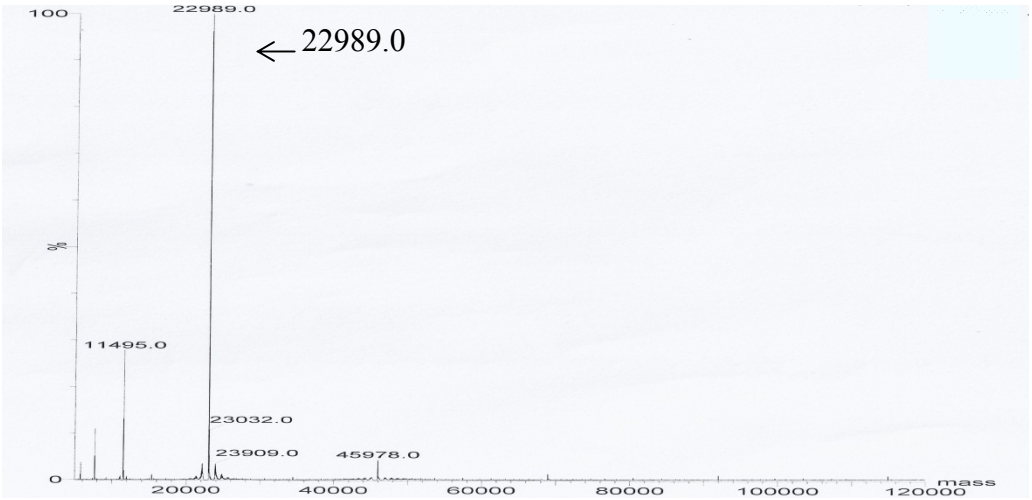

(D)Q217C

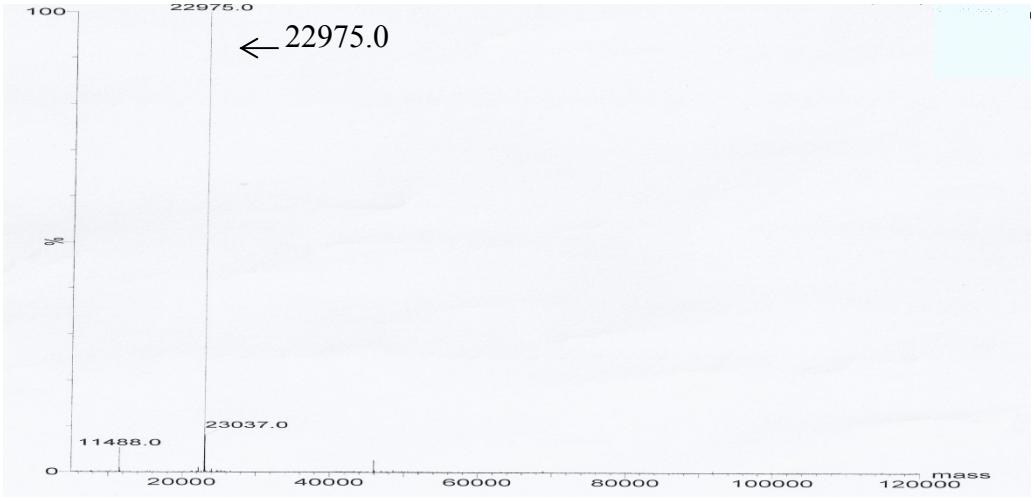

(E)mPrP^{wt}

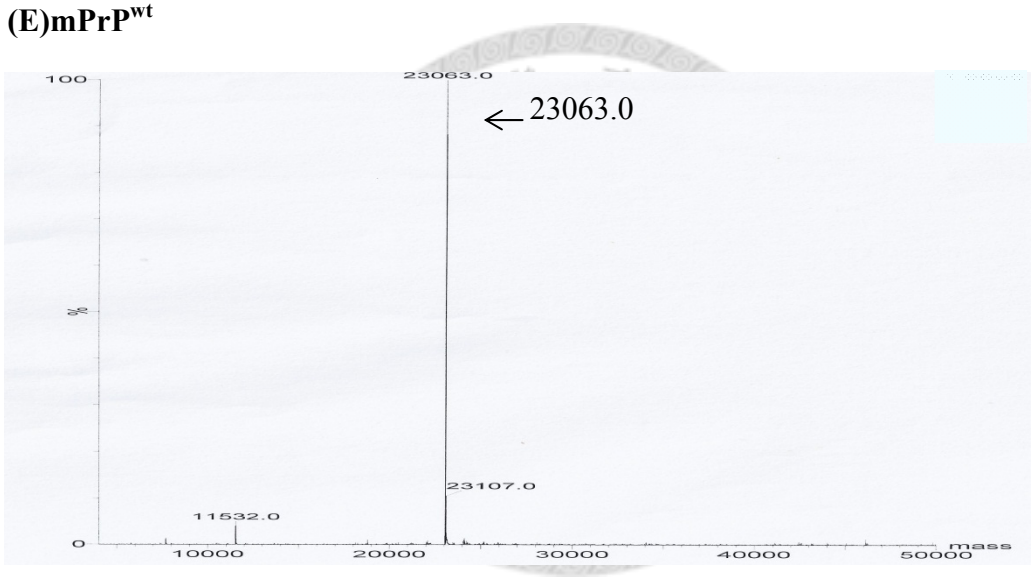

(F)S132R1

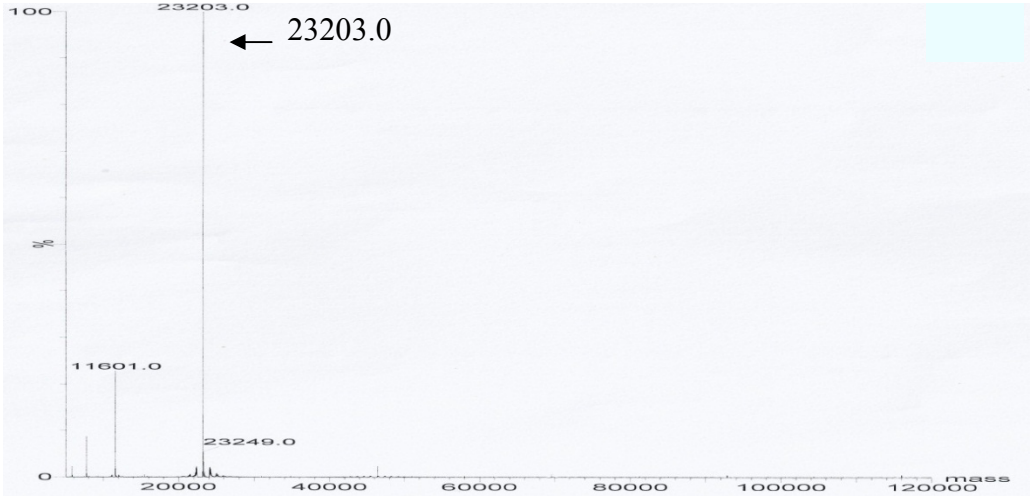

(G)D147R1

(H)N181R1

(I)Q217R1

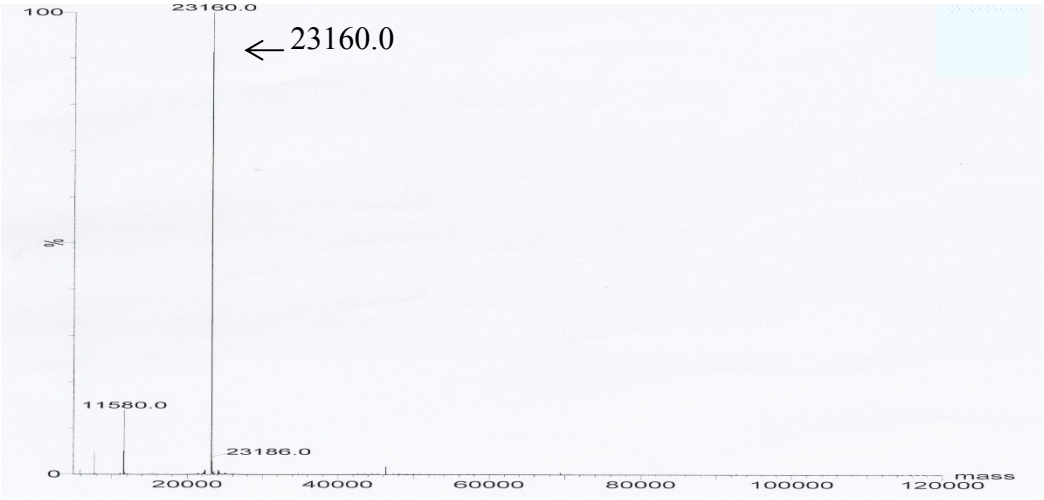

Figure 3.8 ESI-TOF Mass spectra. Mass spectra of S132C, D147C, N181C, Q217C, $mPrP^{wt}$, S132R1, D147R1, N181R1 and Q217R1 were revealed. The corresponding predicted mass for S132C, D147C, N181C, Q217C, $mPrP^{wt}$, S132R1, D147R1, N181R1 and Q217R1 were 23015.4, 22987.3, 22988.3, 22974.3, 23063.4, 23199.7, 23171.6, 23172.6 and 23158.6 Da, respectively. The mass results were coincided with predicted mass.

Chapter 4 Results (II)

4.1 Spontaneous structural conversion under native condition

In our previous study, the disulfide bond-removed PrP can spontaneously proceed structural conversion in 0.5 mM NaOAc, pH 7. Therefore, two newly made constructs including D147C and Q217C also carried out spontaneous structural transition under the same condition. Either CD spectroscopy or ESR spectroscopy was used to monitor the conversion process. Moreover, we found that structural transition rate was slower in a more acidic condition.

4.1.1 CD spectra of spontaneous structural conversion

D147C and Q217C were dissolved in 0.5 mM NaOAc (pH 7.3) and protein concentration was above 0.1 mg/mL. To monitor the structural conversion process, samples were measured by circular dichroism (CD) spectroscopy for more than 2 weeks at room temperature. In order to avoid anything artifact, samples were kept in the CD cuvette and sealed with parafilm during the measurement. And the change of secondary structural contents was analyzed by CDPro software using CDSSTR algorithm. Compared with $mPrP^{wt}$ which contains 29.6 % α-helix, initial CD spectrum of D147C was more disordered and the α-helix content is only 7.6 % (fig. 4.1 A). This indicated that substitution of negative charged aspartate by uncharged cysteine might

destroy the N-capping effect in helix 1. Therefore, D147C was relatively unstable and the structural conversion rate was faster than other mutant PrP. In CD spectra, D147C became more coil-rich within 24 hours. Then it was further shifted to β structure after 100 hours and it finally showed the typical β structure signal on the 281th hour. On the other hand, Q217C showed clearly three-state (α→coil→β) manner of structural conversion (fig. 4.1 B). The secondary structure contents of Q217C were similar to $mPrP^{wt}$ in the beginning and then changed with time (fig. 4.1 D). CD signals of Q217C were changed from α-helix structure to coil-rich structure within 24 hours and were stabilized until 72 hours. The structure had transited to β structure on the 110th hour and it finally became typical β structure on the 405th hour. Although the conversion state of D147C and Q217C were different, they both spontaneously became β structure under native condition. Additionally, proteins aggregated into white precipitations which were visible by eyes after long time incubation.

(A)D147C

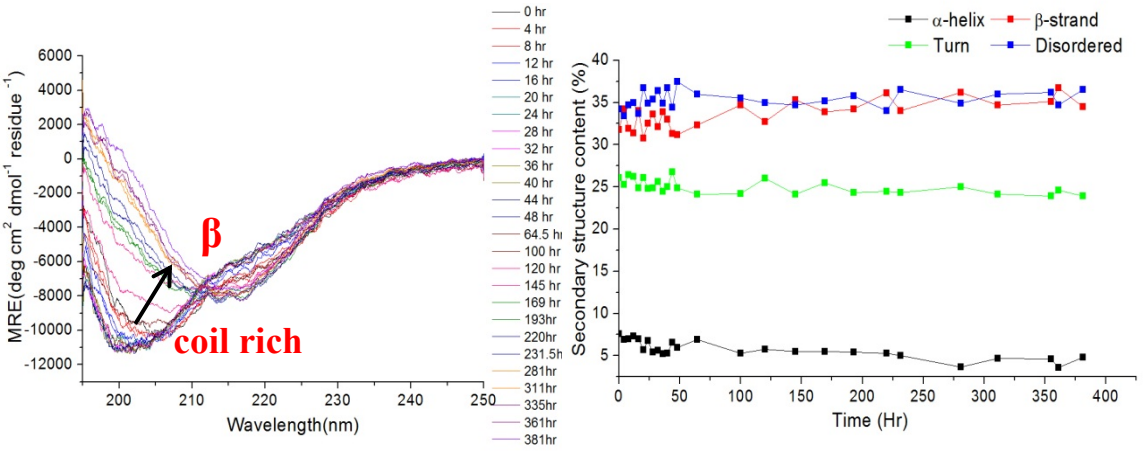

(B)Q217C

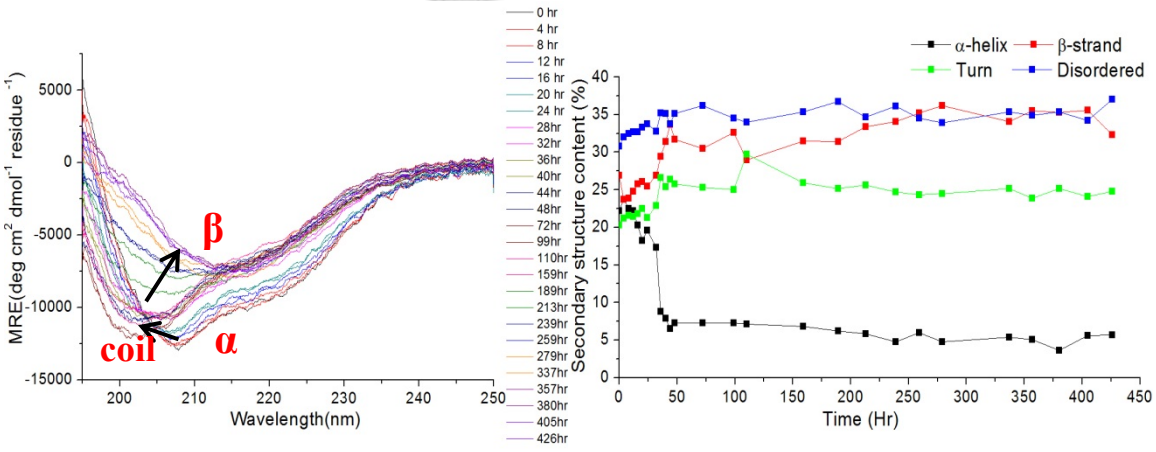

Figure 4.1 Spontaneous structural conversions of D147C and Q217C. (A) D147C and (B) Q217C were dissolved in 0.5 mM NaOAc (pH 7.3) and the structural conversion was monitored by CD. Left panels are the CD spectra. Right panels are variation of secondary over time contents. Q217C showed clearly three state manners. CD signals were deconvoluted by CDPro software using CDSSTR algorithm.

4.1.2 Monitor the spontaneous structural conversion by ESR

After spin-labeling, the spontaneous structural conversion could also be observed by ESR spectroscopy. Since spin motion is very fast, spin labeled sample must be mixed with glycerol or sucrose to slow down the mobility traditionally, so ESR signal can be comprehend. However, previously we found that disulfide bond-removed PrP immediately became β structure after mixed with 40 % sucrose. In order to measure the process of structural conversion, mesoporous silica materials (nanopore) was used to slow down the spin mobility. Nanochannels of mesoporous silica materials are useful for reducing the tumbling motion of encapsulated protein while leaving the biomolecular structure undisturbed (Chaudhary et al, 2008; Lisa Washmon-Kriel, 2000). Moreover, human prion peptide 142-166, which can fold into either a helical or hairpin structure, was studied by ESR within nanopore (Huang & Chiang, 2011). To study spontaneous structural conversion, four different spin-labeled PrP including S132R1, D147R1, N181R1 and Q217R1, were dissolved in 0.5 mM NaOAc (pH 7) and the concentration was about 0.45 mM. And then 20 μL samples were mixed with 12 mg nanopores and were finally measured by ESR spectroscopy for 2 weeks at RT. Exceptionally, the concentration of S132R1 was only 0.27 mM, so we added 30 μL into nanopores.

To ensure that the PrP structure had changed within nanopores, we measured all the samples initially and after 2 weeks by CD spectroscopy (fig. 4.2). S132R1 showed α-helix signal at first and further became β structure after 2 weeks within nanopores. However, the CD spectra of other three mutant PrP showed hybrid signals, indicating that some proteins had already been transformed into β structure at the beginning. According to the CD intensity, the protein concentration of N181R1 should be lower compared with other mutant PrP. After 2 weeks, the CD signals were slightly different and the intensity decreased. Nevertheless, ESR spectra showed obvious differences after 2 weeks, suggesting that the structures were altered (fig. 4.3). ESR signals can be divided into two components – fast and slow. The intensity of fast component in all spin-labeled PrP had increased with time, indicating that the backbone of PrP was more relaxed and the conformation dynamic had increased. Therefore, mutant PrP became more flexible during the structural conversion under native condition (0.5 mM NaOAc, pH 7). On the other hand, the slow component was correlated with environment of spin-labeled residue. For ESR spectra of S132R1, slow component was not affected by structural conversion, suggesting that this residue was not involved in the association process. Slow component in N181R1 spectra was also unchanged, but we expected that helix 2 was partially unfolded in β-oligomers structure. The total protein of N181R1 was less than others, so N181R1 may need more time for association.

Moreover, the slow component of D147R1 increased after 250 hours, indicating that residue 147 may involve in the structural conversion and the oligomers association process. Interestingly, the Q217R1 spectrum showed inter-spin interaction at the beginning and the interaction had increased gradually with time. Therefore, Q217R1 started to aggregate into oligomers in the beginning and residue 217 may locate at the intermolecular association region.

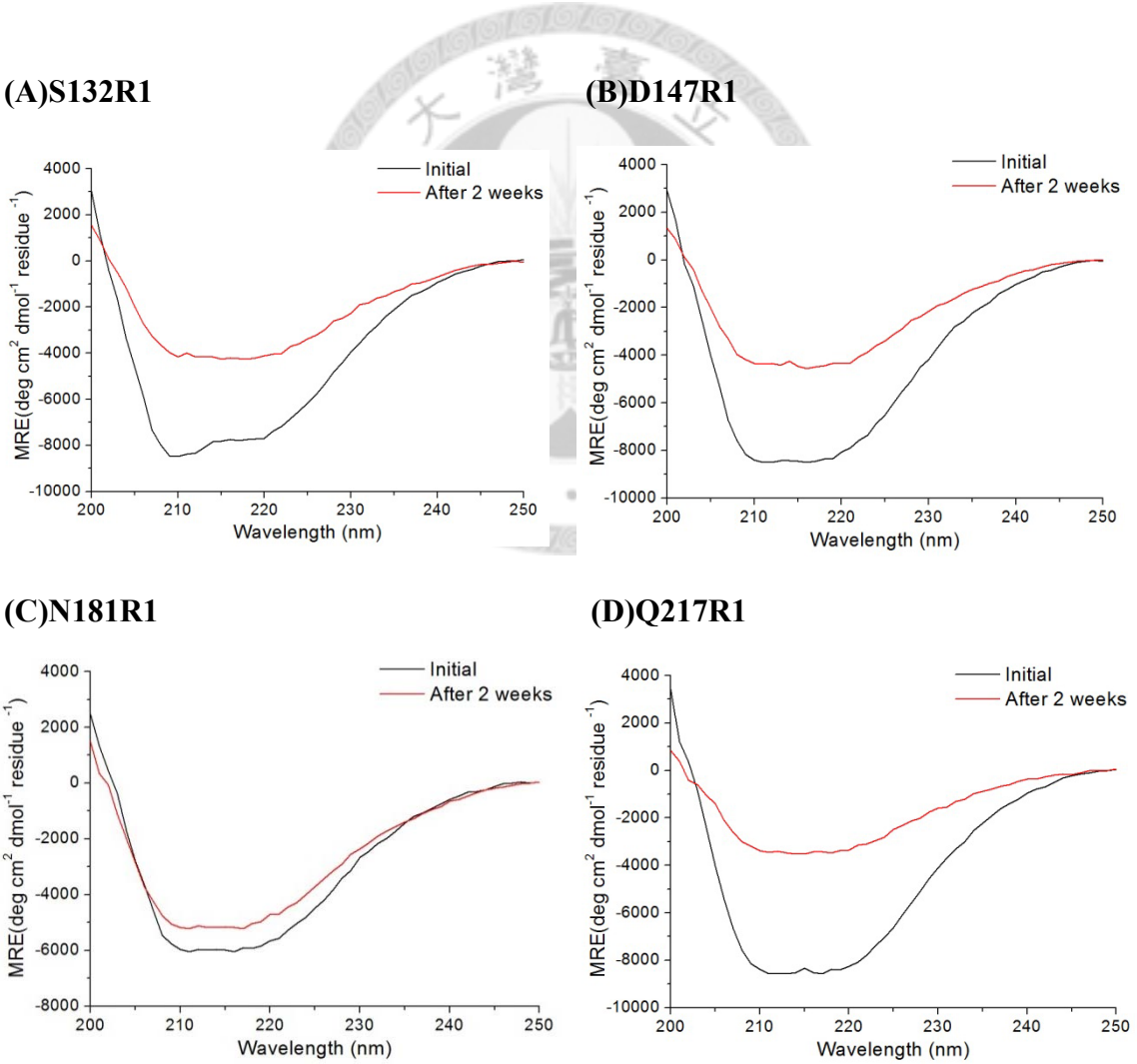

Figure 4.2 CD spectra of different spin-labeled PrP within nanopores. S132R1, D147R1, N181R1 and Q217R1 were dissolved in 0.5 mM NaOAc (pH 7) within nanopores. CD spectra were measured initial (red) and after 2 weeks (black).

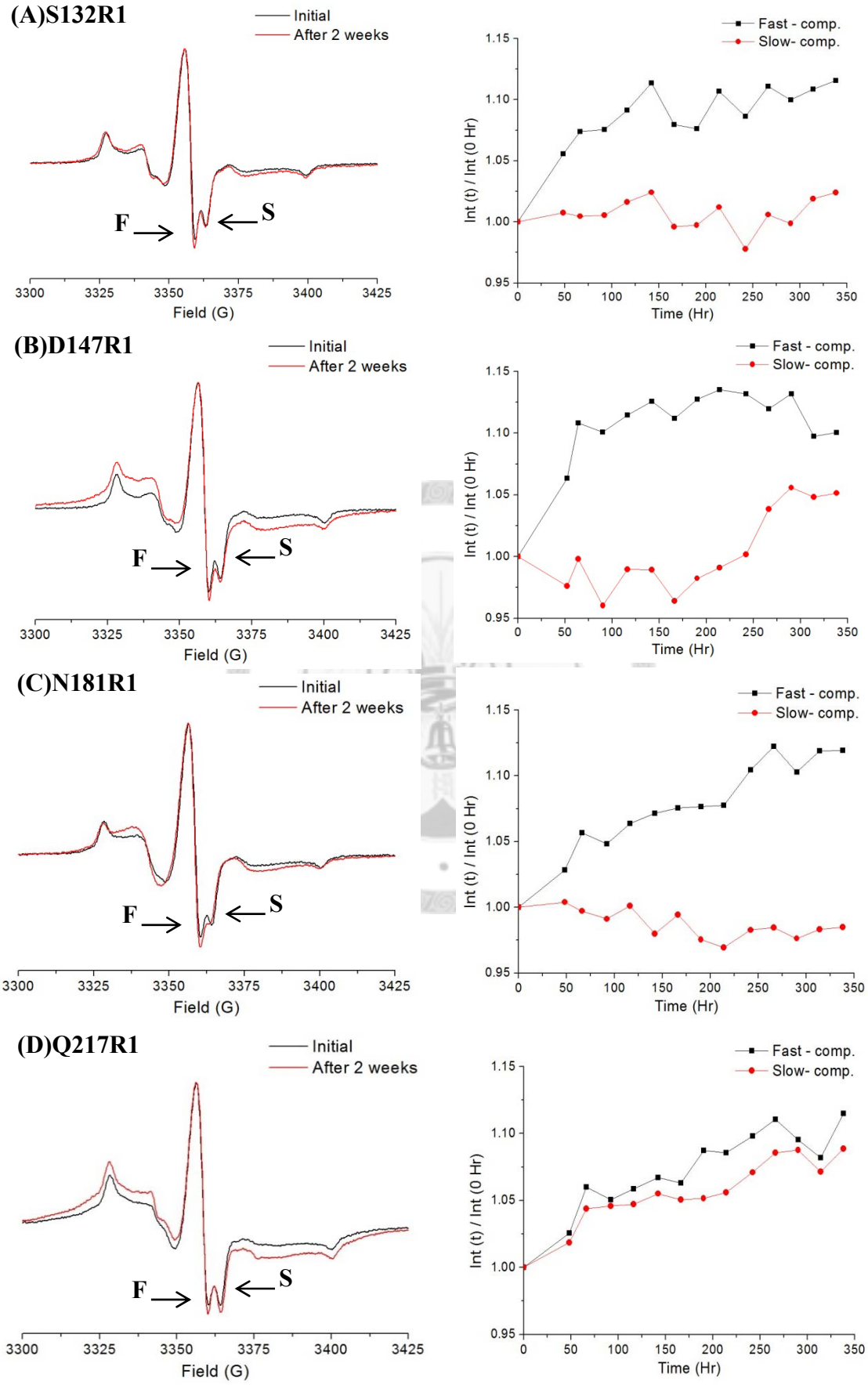
(A)S132R1
Initial
After 2 weeks
F
S
Field (G)
Fast - comp.
Slow- comp.
Int (t) / Int (0 Hr)
Time (Hr)
(B)D147R1
Initial
After 2 weeks
F
S
Field (G)
Fast - comp.
Slow- comp.
Int (t) / Int (0 Hr)
Time (Hr)
(C)N181R1
Initial
After 2 weeks
F
S
Field (G)
Fast - comp.
Slow- comp.
Int (t) / Int (0 Hr)
Time (Hr)
(D)Q217R1
Initial
After 2 weeks
F
S
Field (G)
Fast - comp.
Slow- comp.
Int (t) / Int (0 Hr)
Time (Hr)

Figure 4.3 Spontaneous structural conversions of ESR spectrum within nanopores. The ESR signals of (A) S132R1, (B) D147R1, (C) N181R1 and (D) Q217R1 in 0.5 mM NaOAc (pH 7) within nanopores. Left panels are ESR spectra initial and after 2 weeks. Black arrows indicate fast component and slow component. Right panels show the change of fast and slow components with time.

4.1.3 pH value can affect structural conversion rate

We found that mutant PrP in 0.5 mM NaOAc with different pH value caused different structural conversion rate. D147C and Q217C were dissolved in an acidic condition (0.5 mM, pH 5.6) at room temperature. However, spontaneous structural conversion process became slower and even longer than one month (fig. 4.4). Compare with fig. 4.1 (pH 7.3), D147C was more stable at pH 5.6 and the α-helix content increased to 19.4 % at the beginning. Based on the CD spectra of D147C in acidic condition, we observed that the transition time from α-helix to coil-rich structure was delayed to 6 days and it required more than 40 days to convert into β structure. In addition, Q217C also carried out slower transition rate under an acid condition. The α-helix content gradually decreased in 23 days after incubation and then CD signal changed to β structure on the 44^{th} days. In order to investigate this phenomenon, double mutant PrP, S132C/N181C, was used because it has the fastest structural conversion rate. S132C/N181C was dissolved in 0.5 mM NaOAc with different pH values including pH 6.5, pH 5.9 and pH 5.3, and then was incubated within CD cuvettes

at room temperature. The results of the time course from CD spectra were shown in fig. 4.5. Obviously, the structure transformed slower in the acidic conditions and was pH-dependent. For pH 6.5 condition, the structure was changed after 1 day and α-helix content also decreased. Different from the pH 6.5 condition, in pH 5.9 and pH 5.3 conditions, the conversion rates were slower and α-helix content decreasing times were prolonged to 2 days and 4 days, respectively. These results confirmed that pH value was important for spontaneous structural conversion and this process was pH-dependant.

(A)D147C

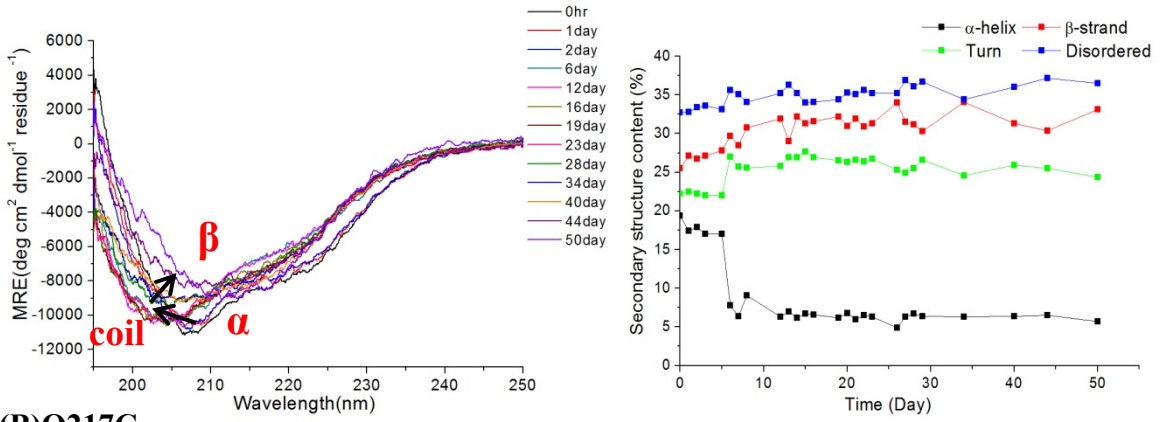

(B)Q217C

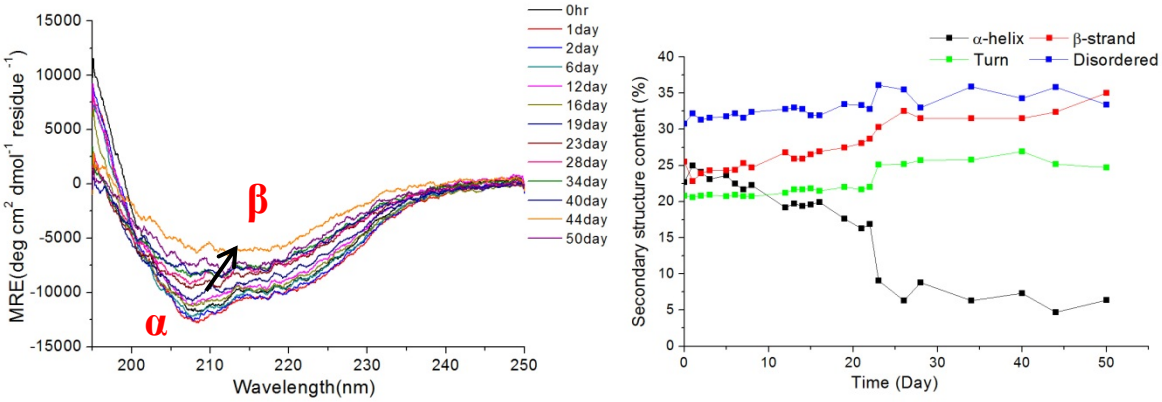

Figure 4.4 Spontaneous structural conversions of D147C and Q217C under acidic condition. (A) D147C and (B) Q217C were dissolved in acid condition (0.5 mM NaOAc, pH 6.5) and were monitored by CD. Left panels are the CD spectra. Right panels are variation of secondary over time contents. Both showed slower structural conversion rates. CD signals were deconvoluted by CDPro software using CDSSTR algorithm

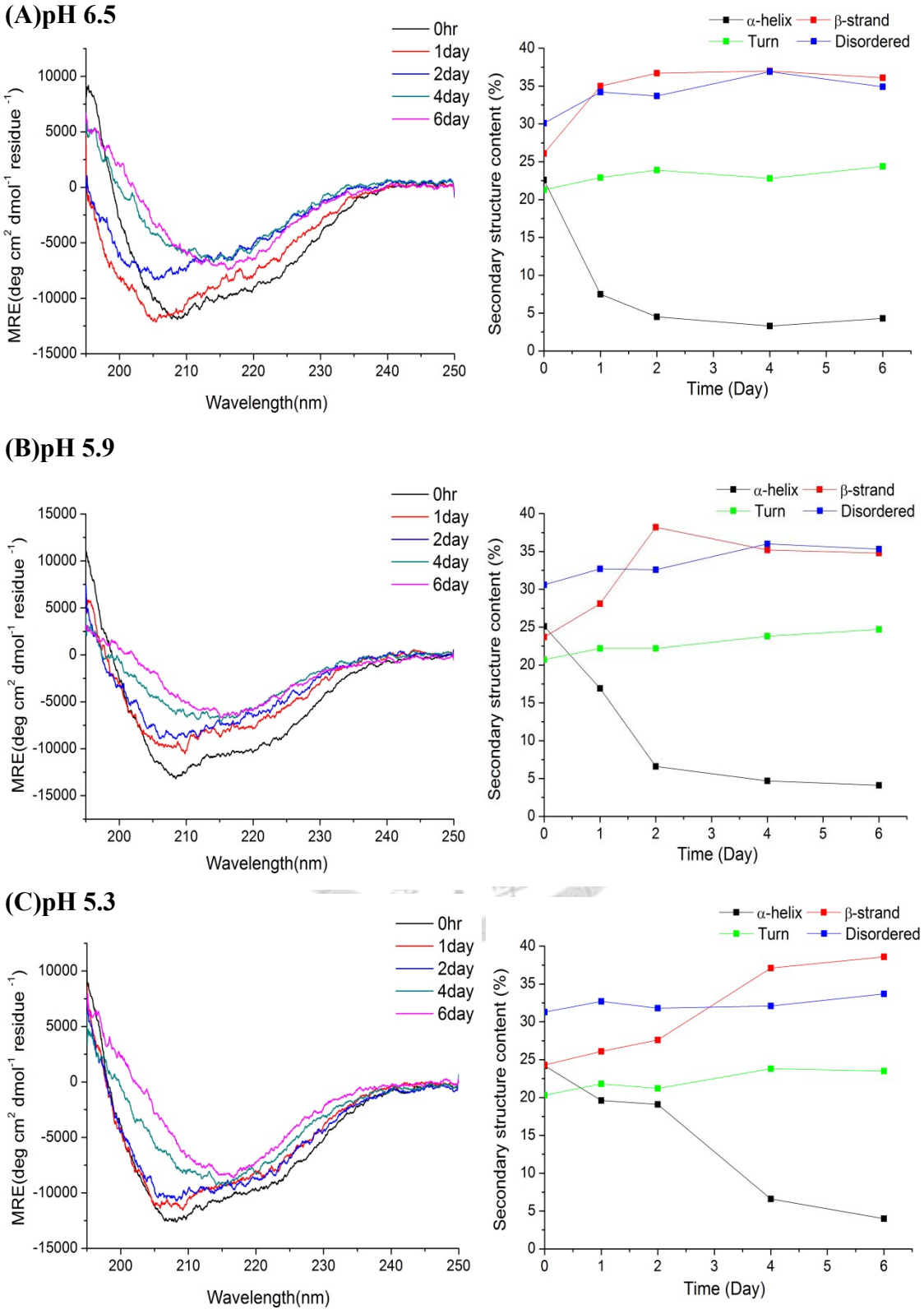

Figure 4.5 Spontaneous structural conversion of S132C/N181C under different condition. S132C/N181C was dissolved in 0.5 mM NaOAc with different pH value. (A) pH 6.5. (B) pH 5.9. (C) pH 5.3. Left panels were CD spectrum by time. Right panels were deconvoluted by CDPro software using CDSSTR algorithm. More

acid, the structural conversion rate was slower.

4.2 Soluble β-PrP

According to our previous study, disulfide bond-removed PrP dissolved in higher salt concentration buffer (10 Mm NaOAc) can immediately transit to β-structure. In addition, analytic ultracentrifugation (AUC) and transmission electron microscopy (TEM) both showed that β-PrP was oligomers. D147C and Q217C were dissolved in 10 mM NaOAc and we also used AUC and TEM to assure that they can form β-oligomers. And then, we measured the spin-labeled β-PrP by ESR spectroscopy. The ESR spectra from different regions may provide some structural information about β-PrP.

4.2.1 CD spectra of β-PrP

D147C and Q217C were dissolved in 10 mM NaOAc (pH 7) and the concentration was about 0.1 mg/mL. Although CD spectra were slightly different from D147C and Q217C, they both showed typical β signals which had negative signals around 218 nm (fig. 4.6). The results were consistent with that the disulfide bond-removed PrP can form β-structure under native condition in higher salt concentration.

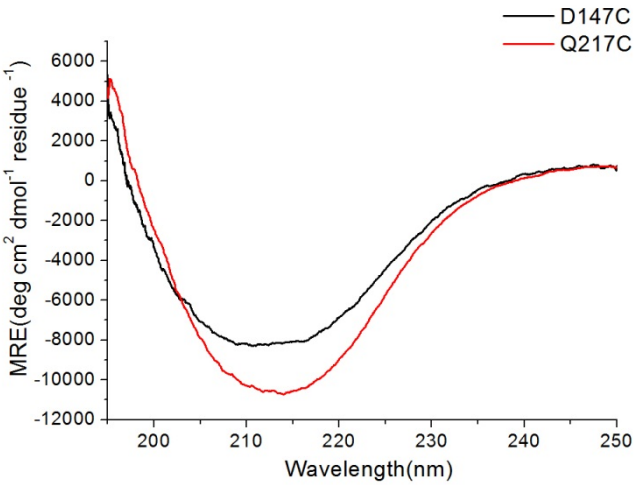

Figure 4.6 β-PrP can form in 10 mM NaOAc. D147C and Q217C were dissolved in 10 mM NaOAc (pH 7) and the concentration was about 0.1 mg/mL. Far-UV CD spectra revealed a predominant β-sheet pattern.

4.2.2 Particle size determination

Then we examined the aggregation propensity of β-PrP by analytic ultracentrifugation (AUC). D147C and Q217C were freshly prepared in 10 mM NaOAc buffer (pH 7) and were subjected to sedimentation velocity analytic ultracentrifugation (SV-AUC). The sedimentation coefficient distributions showed that β-PrP did not sediment as a single species but as a mixture of oligomers (fig. 4.7). AUC spectra suggested that D147C and Q217C still contained some monomer with a sedimentation coefficient of ~2 S, but the oligomers distribution were different. The major peaks of D147C corresponded to 15-16 mer and 25 mer, respectively. In contrast, the major peaks of Q217C corresponded to 10-11 mer, 21-22 mer and 33-34 mer, respectively. AUC results confirmed that D147C and Q217C did formed

β-oligomers. Interestingly, the intervals of different population oligomers were all about 10 mer.

(A)D147C

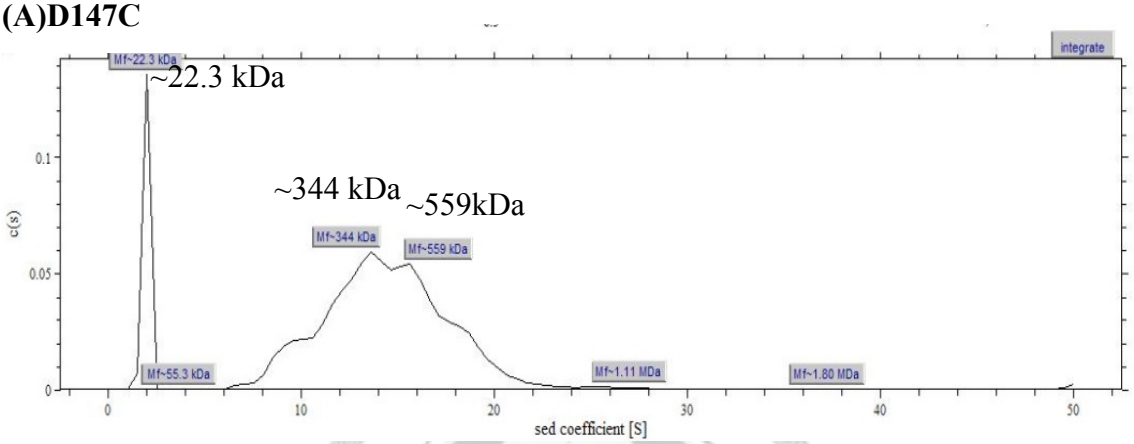

(B)Q217C

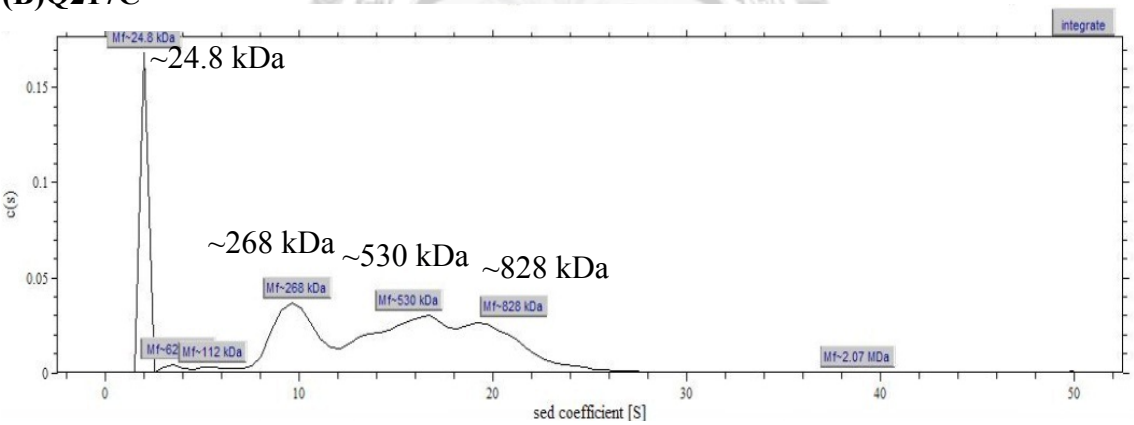

Figure 4.7 Analytical ultracentrifugation. Continuous c(s) distribution characterizes the sedimentation coefficient of D147C and Q217C in 10 mM NaOAc buffer (pH 7.0). Scans were acquired using absorbance at 280 nm.

4.2.3 TEM image and ThT assay of β-PrP

The β-PrP morphology of D147C and Q217C were visualized by transmission electron microscopy (TEM). They were dissolved in 10 mM NaOAc buffer (pH 7) as well but with lower protein concentration (0.08 mg/mL). We found that this

concentration promoted oligomers formation. TEM images of D147C and Q217C both showed bead-like morphology (fig. 4.8). The bead-like morphology is the characteristic of oligomers. As same as the AUC results, we can found different sizes of beads. Therefore, either AUC results or TEM images disclosed oligomer formation under native condition with higher salt concentration.

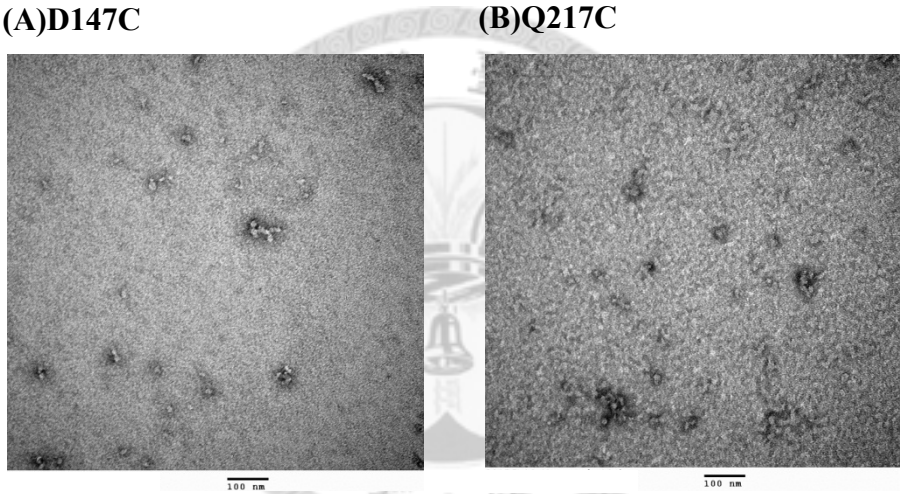

Figure 4.8 TEM images of D147C and Q217C oligomers. D147C and Q217C oligomers were negative-stained by using 2 % (w/v) uranyl acetate. TEM images revealed bead-like morphology. The bar represents 100 nm.

In previous study, β-PrP oligomers showed high intensity on thioflavin T (ThT) binding assay. ThT is a well-used indicator of amyloid fibrils. Its non-specific binding emits fluorescence around 480 nm under excitation at wavelength of 420 nm. As shown in fig. 4.9, D147C and Q217C β-PrP oligomers displayed high fluorescence signals similar to previous construct S132C/N181C. This indicated that β-PrP formed

a plenty of ThT-binding β-sheet.

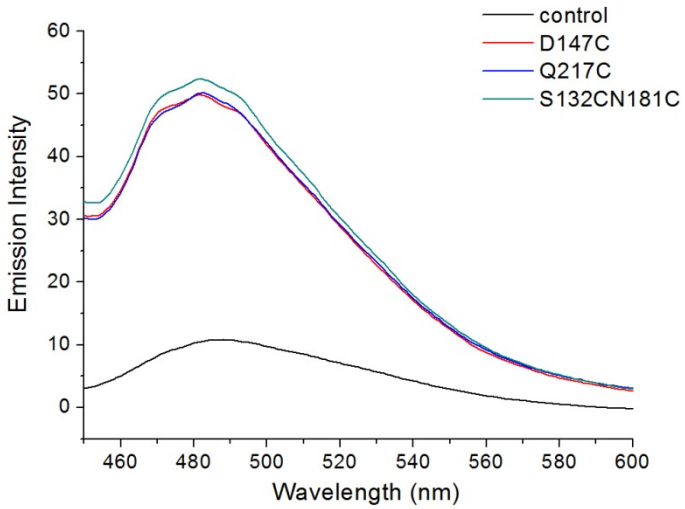

Figure 4.9 ThT binding assay of different mutant PrP. Mutant PrP oligomers were formed in 10 mM NaOAc buffer (pH 7) and mixed with ThT solution. β-PrP oligomers showed high intensity. Fluorescence was detected with excitation at 420 nm. DI water was mixed with ThT solution for control.

Interestingly, the β-PrP oligomers became fibril structure after long time incubation at room temperature without shaking. After one month, β-PrP samples were examined by TEM again. However, TEM images revealed fibrils morphology (fig. 4.10). This finding suggested that disulfide bond removed PrP can form amyloid fibrils under native condition without any denaturant agents. Moreover, ThT intensity did not increase after fibril formation (data not shown). The possible explanations are that the fibrils concentration is not enough to be detected or the fibrillization process started from β-oligomers is unable to form more ThT-binding β-structures. These results indicated that oligomers may be the precursor of fibrils and they gradually form

fibril after long time incubation.

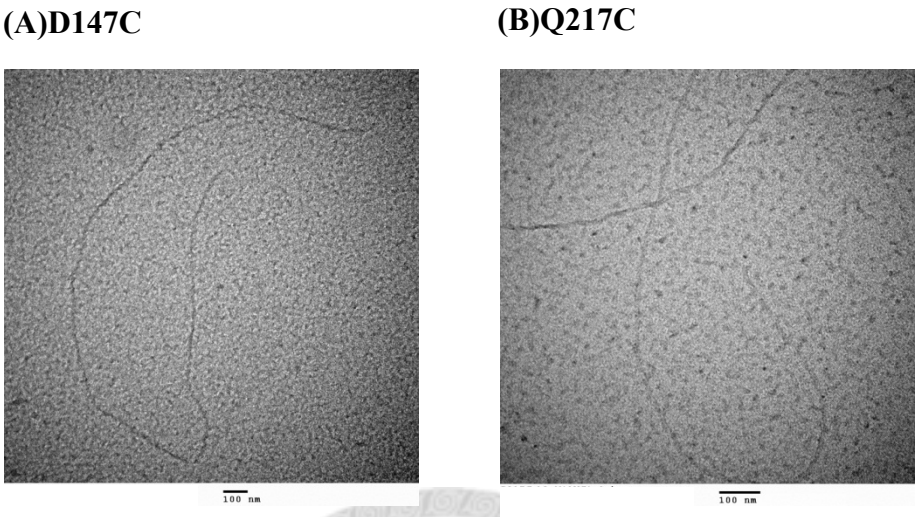

Figure 4.10 TEM images revealed fibrils after long time incubation. D147C and Q217C oligomers were incubated more than one month at room temperature. Negative-stained was done by using 2 % (w/v) uranyl acetate. TEM images revealed fibrils morphology. The bar represents 100 nm

4.2.4 ESR spectra of β-PrP

To further investigate the structural details in β-PrP aggregation, different mutant PrP were labeled with MTSSL and were measured by ESR spectroscopy. D147R1 and Q217R1 were dissolved in 10 mM NaOAc buffer (pH 7) and the concentration was 0.45 mM. And then, samples were mixed with 40 % sucrose and measured at 300 K. The results were shown in fig. 4.11 and were combined with previous data, S132R1 and N181R1. For S132R1, which spin-labeled site on loop, the ESR signal indicated that residue-132 in soluble β-PrP remained highly flexible. In the native structure, residue D147, N181 and Q217 are located at helix 1, helix 2 and helix 3, respectively.

According to the ordered structure of helix, their ESR signal should present slow motion. However, the ESR signals of D147R1 and N181R1 contained slow and fast ESR spectral components, indicating that helix 1 and helix 2 were partially unfolded during the β-PrP formation. On the other hand, spin labeled on helix 3 showed slow mobility, suggesting that the local environment of that spin is in an ordered state. Moreover, the dipole-dipole interaction between two spin labels is insignificant, suggesting that the inter-spin distance is greater than the upper limit of CW-ESR (~2 nm).

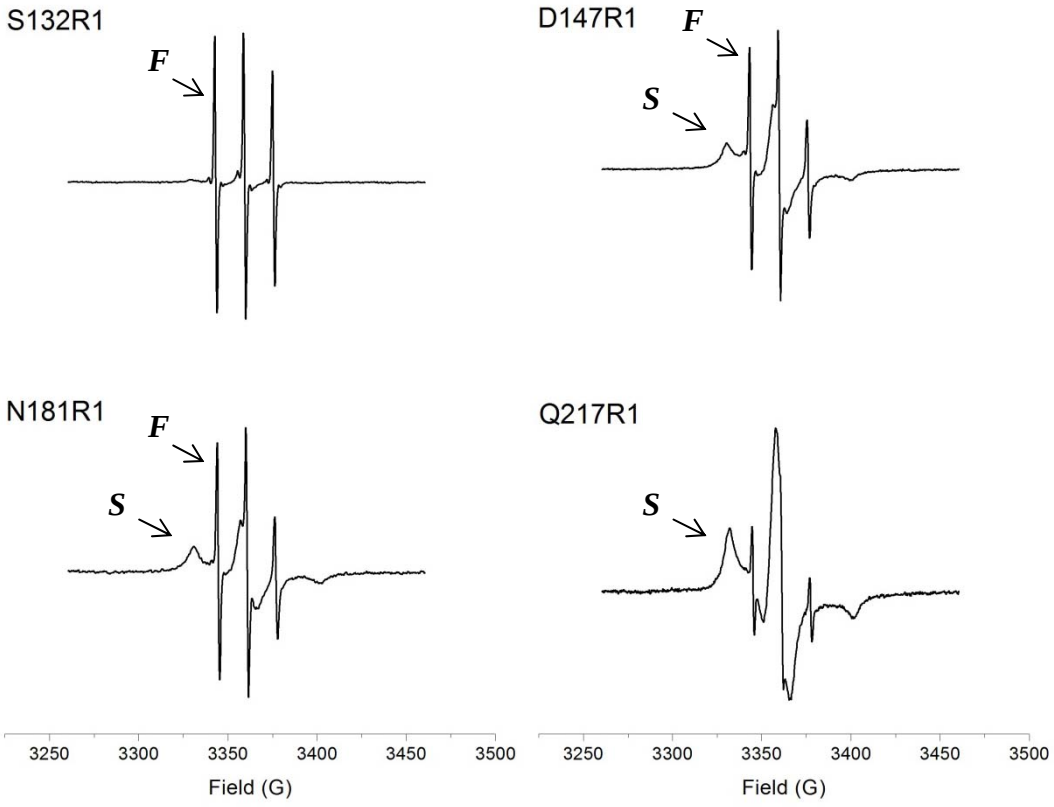

Figure 4.11 ESR spectra of β-PrP. The labeled proteins (0.45 mM) were measured

in 10 mM NaOAc buffer (pH 7.0) containing 40 % sucrose under 300K. Four different spin-labeled region of mutant PrP are shown. S132R1 and N181R1 results come from previous study. The arrow with ***F*** denotes the fast component in spectrum, and the arrow with ***S*** denotes the slow component.

4.3 Amyloid fibrils

In vivo, PrP^{Sc} aggregates in brain tissues and shows amyloid fibril-like structure. Therefore, fibrillization process and amyloid fibril structure are important aspects for PrP^{Sc} infection. Many reports have proposed that recombinant mPrP can form amyloid fibrils under denaturing condition in vitro and the morphology is similar to native fibrils (Bocharova et al, 2005). In our study, fibrils were produced from different mutant PrP under denaturing condition and the process was detected by ThT binding assay. TEM revealed the morphology of different amyloid fibrils. Moreover, ESR spectroscopy and pepsin digestion assay were used to further study fibril structure.

4.3.1 ThT binding assay and TEM images of mutant PrP

Under partially denaturing condition (1 M GdnHCl, 3 M urea, PBS, pH 7), mutant PrP was transformed into amyloid fibrils and the process can be detected by the ThT binding assay. The protein concentration was about 22 μM and incubated in 37 ℃ incubator with 250 rpm shaking for several days. The emission fluorescence intensity of ThT was measured by excitation at wavelength of 420 nm with time. All mutant

PrP were visible to the eyes when they reached the equilibrium state. Fig. 4.12 showed the time course of fluorescence intensity at 487 nm of the following proteins, S132C, D147C, N181C, Q217C and $mPrP^{wt}$. Every disulfide bond-removed PrP had shorter lag time than wildtype PrP. According to nucleation model, the disulfide bond-removed PrP was unstable and easily formed amyloid seeds. Besides, the mutant PrP had slightly faster elongation rate, except Q217C, which had slower elongation rate.

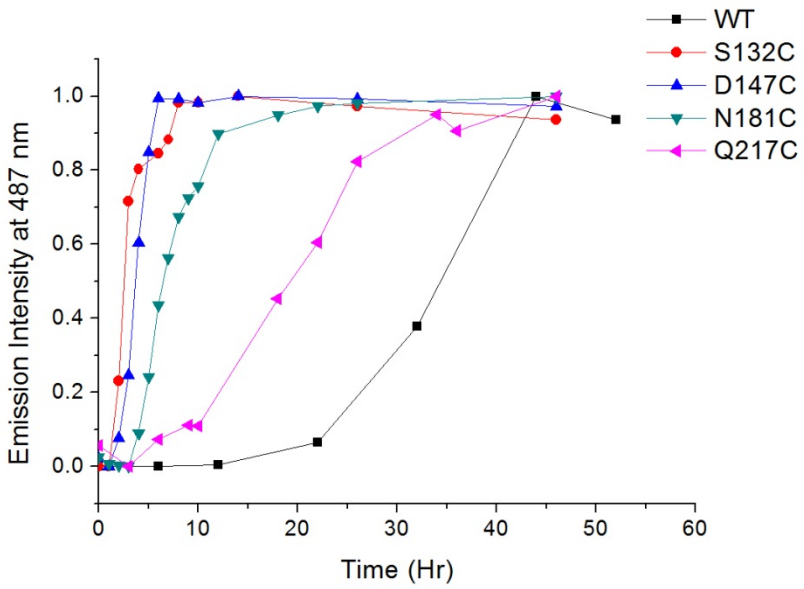

Figure 4.12 Fibrillization process of different mutant PrP. 22 μM mutant PrP was keep in partially denaturing condition (1 M GdnHCl, 3 M urea, PBS, pH 7) and incubated in 37 ℃ incubator with 250 rpm shaking. Samples were measured by ThT assay until reached the equilibrium state. Different colors represent different mutant PrP. Fluorescence was detected with excitation at 420 nm. Y axis represents the normalized results of emission intensity at 487 nm.

In addition, the morphology of every mutant PrP fibril was visualized by transmission electron microscopy (TEM). The length of amyloid fibrils can be longer

than 1 μm. The morphology of these fibrils was similar except Q217C which showed more twisted fibrils (fig. 4.13).

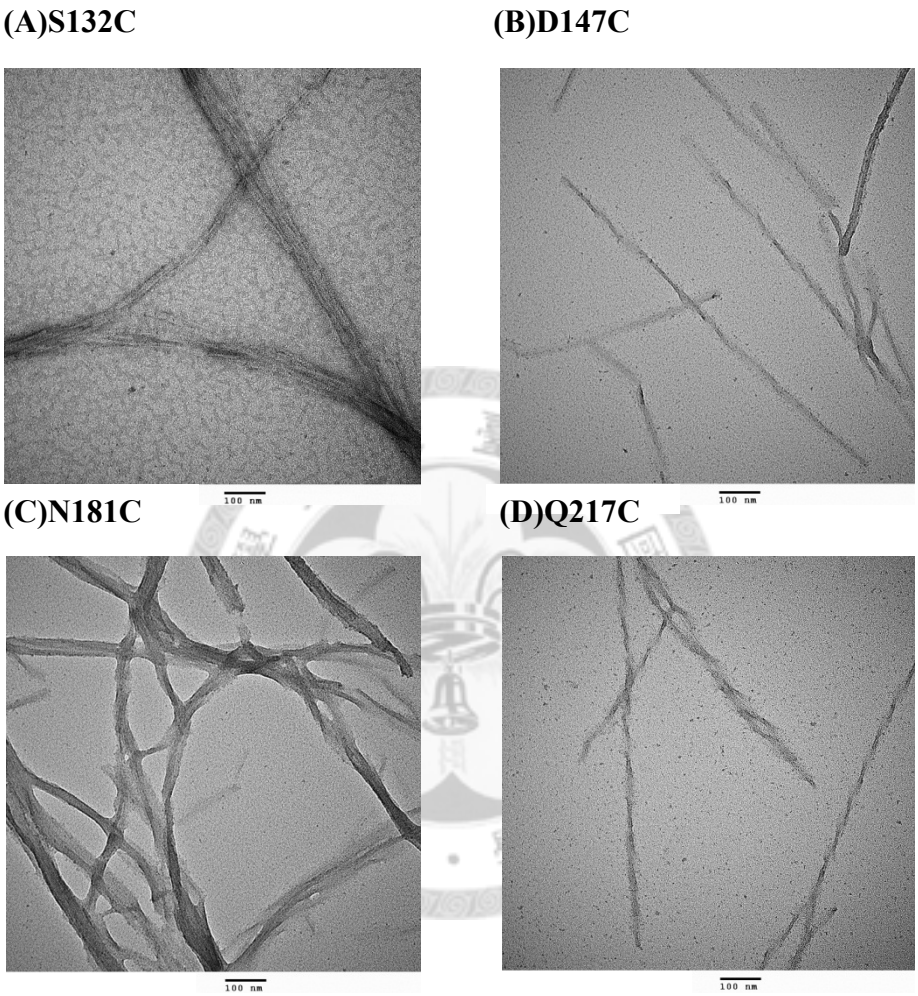

Figure 4.13 TEM images of different fibrils. Under partially denaturing condition (1 M GdnHCl, 3 M urea, PBS, pH 7), the mutant proteins were transformed into amyloid fibrils. Negative-stained was done by using 2 % (w/v) uranyl acetate. Morphology of these fibrils was similar except Q217C showed twisted structure. The bar represents 100 nm.

4.3.2 Fibrils formed from Spin-labeled PrP

Spin-labeled PrP can form amyloid fibril under a partially denaturing condition as well. The same fibrillization procedure was used and the time course data of different MTSSL-labeled PrP was monitored by ThT binding assay (fig. 4.14). The lag time of different spin-labeled PrP was similar to fig 4.12, indicating that the spin-label probe did not affect the amyloid seed formation. Interestingly, the N181R1 had the slowest elongation rate, implying that the R1 group on residue 181 might interfere with the association between monomer and existing fibrils.

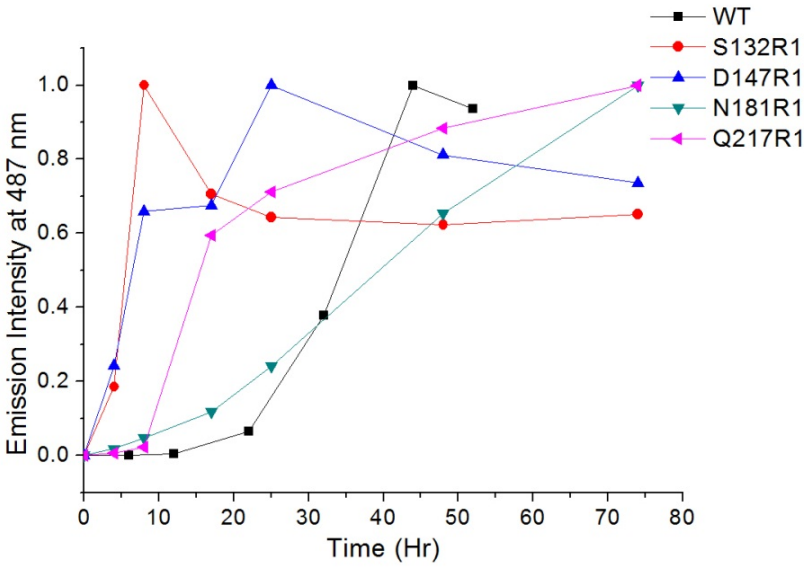

Figure 4.14 Fibrillization process of different spin-labeled PrP. 22 μM different mutant PrP were dissolved in partially denaturing condition (1 M GdnHCl, 3 M urea, PBS, pH 7) and incubated in 37 ℃ incubator with 250 rpm shaking. Samples were measured by ThT assay until reached the equilibrium state. Different colors represent different mutant PrP. Fluorescence was detected with excitation at 420 nm. Y axis represents the normalized results of emission intensity at 487 nm.

Spin-labeled fibrils were observed by TEM likewise. As shown in fig. 4.15, spin-labeled fibrils had similar morphology as fig 4.14. This suggested that the fibril structure is not affected by MTSSL labeling. In the same manner, the morphology of these fibrils was similar except Q217R1, which showed clearly twisted structure. No matter Q217C or Q217R1 showed more twisted fibrils, suggesting Q217 plays a role on association.

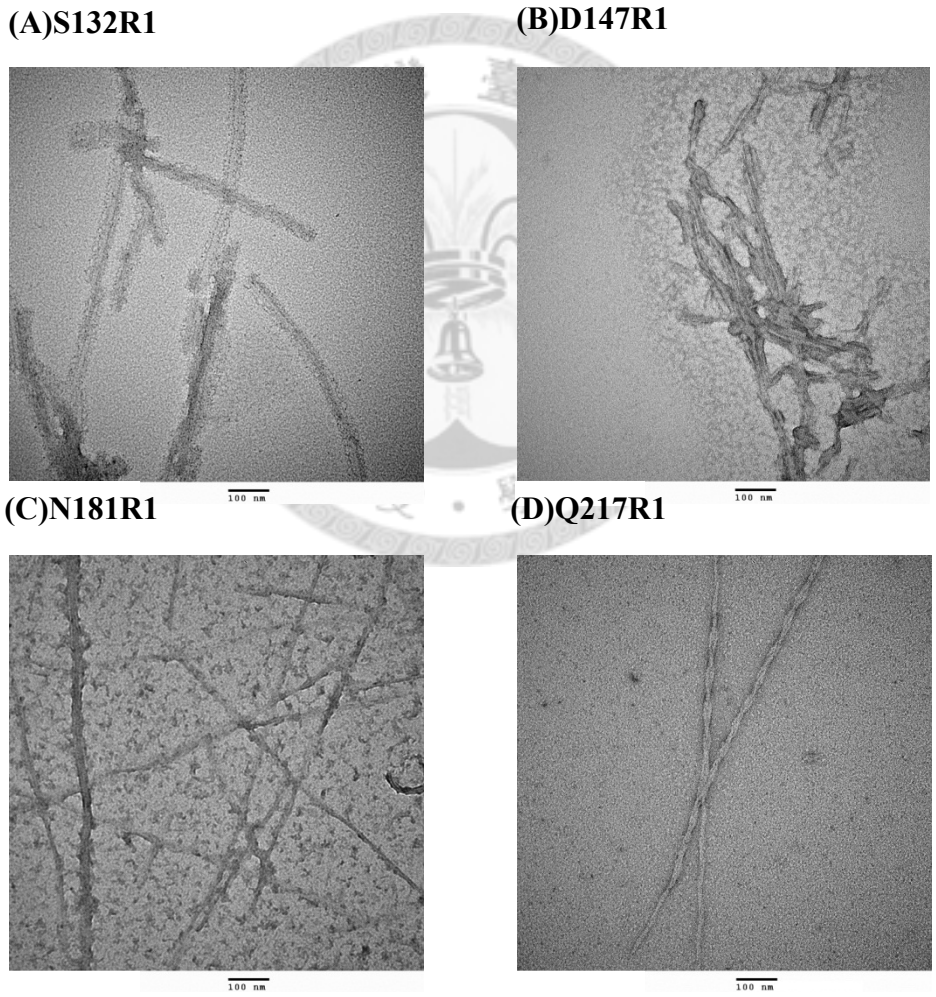

Figure 4.15 TEM images of spin-labeled fibrils. Under partially denaturing condition (1 M GdnHCl, 3 M urea, PBS, pH 7), the spin-labeled PrP were transformed into amyloid fibrils structure. Negative-stained was complete by using 2 % (w/v) uranyl acetate. The morphology of these fibrils was similar except Q217R1 showed

clearly twisted structure. The bar represents 100 nm.

4.3.3 ESR spectra of amyloid fibrils

Furthermore, spin-labeled fibrils were mixed with 40 % glycerol and were measured by ESR spectroscopy at 200 K. The results were shown in fig. 4.16. Compared to the ESR spectra in fig. 4.11, the ESR signals from fibrils sample were much broader and had slower motion. The variation came from more compacted structure of amyloid fibrils and from lower experimental temperature. The ESR spectra of S132R1 and D147R1 showed flexible signals, suggesting that the residue 132 and 147 are in a flexible region in fibril structure. On the other hand, the ESR signals of N181R1 and Q217R1 showed slow mobility, suggesting that residues 181 and 217 are in an order state while PrP becomes fibril structure. The ESR spectra of Q217R1 fibrils showed intermolecular spin interaction with a distance of 10 Å. This is very short distance and it indicated that there may be a regular space between residue-217s of different PrP molecules.

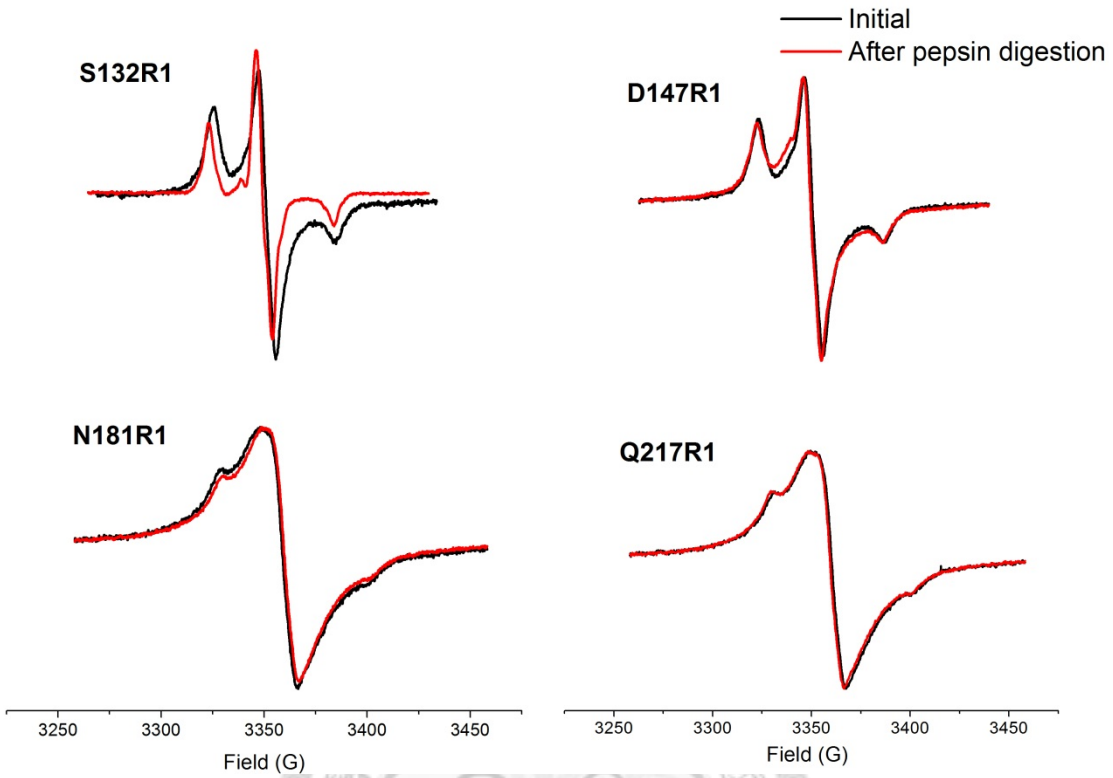

Figure 4.16 ESR spectra of MTSSL-labeled fibrils initial and after pepsin digestion. The spin-labeled fibrils were mixed with 40 % glycerol and measured by ESR spectroscopy at 200 K. S132R1 and D147R1 show flexible signals and change after pepsin digestion. The ESR signals of N181R1 and Q217R1 showed slow mobility and were not affected by pepsin digestion. Black lines represent the initial ESR spectra and red lines represent the ESR spectra after pepsin digestion.

4.3.4 Pepsin digestion assay

To investigate which residue is involved in amyloid core, we digested the spin-labeled fibrils by pepsin. Pepsin was chosen because of its broad specificity. The cleavage sites are not dictated by the amino acid sequence, but by the conformational and dynamical features of the polypeptide chain (Hooper, 1990). Pepsin digestion has been used to identify the amyloid core of lysozyme fibrils (Frare et

al, 2006). Additionally, pepsin has never been used for prion fibrils digestion, but proteinase K has been used before (Bocharova et al, 2005). Our idea is that if the residue is not involved in amyloid core, the residue can be cut off by pepsin and the ESR signal will change. Therefore, spin-labeled fibrils were digested for more than 30 min at room temperature with pepsin at an Enzyme: Substrate ratio of 1:15 (w/w) in the acidic condition (10 mM HCl). The ESR spectra were measured at 200 K and shown in fig. 4.16. TEM images revealed that all fibrils became shorter after pepsin digestion (fig 4.17). The ESR signals of S132R1 changed significantly after pepsin digestion, suggesting that residue 132 might be cut out from amyloid fibrils by pepsin. Residue 132 might be either not in the amyloid core or in a loop. For D147R1, N181R1 and Q217R1, the spectra were not significantly changed before and after pepsin digestion, indicating that residue 147, 181 and 217 are in an ordered state and are not exposed.

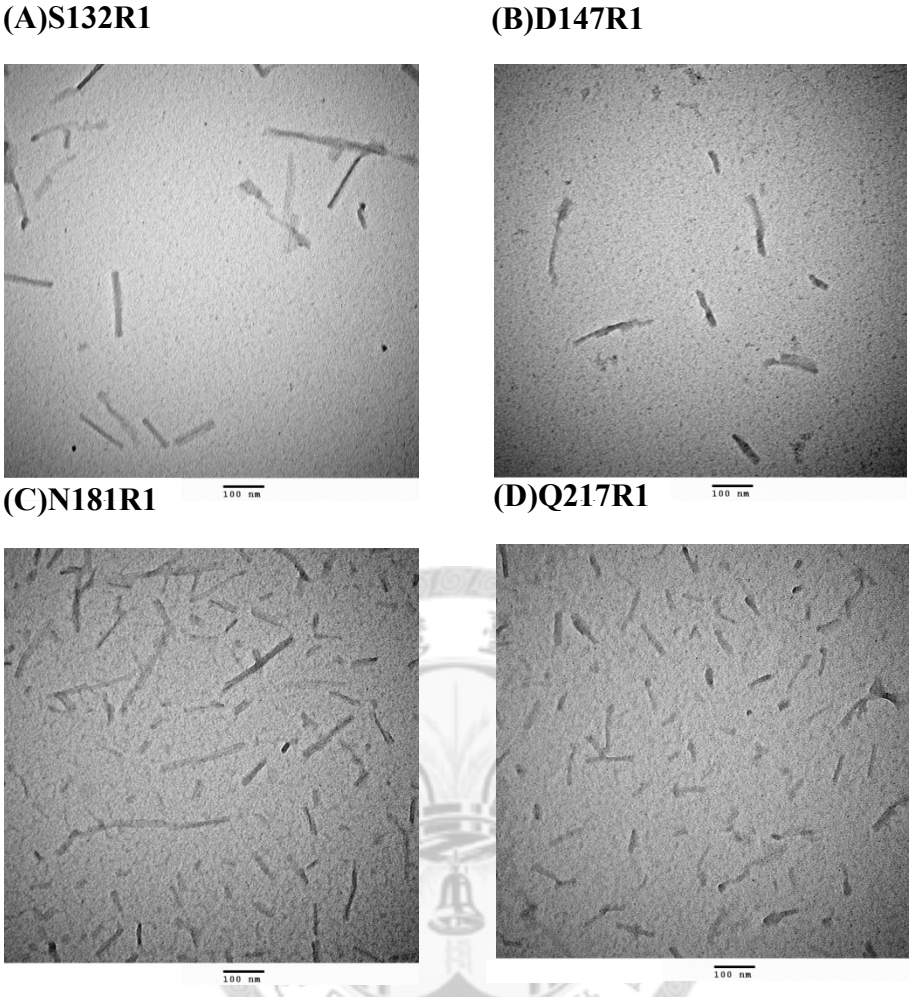

Figure 4.17 TEM images of spin-labeled fibrils after pepsin digestion. The spin-labeled fibrils were digested for more than 30 min at room temperature with pepsin at an E:S ratio of 1:15 (w/w) at acid condition (10 mM HCl). Negative-stained was done by using 2 % (w/v) uranyl acetate. The morphology of these fibrils became shorter after pepsin digestion. The bar represents 100 nm.

Chapter 5 Discussion

The conversion of natural prion protein (PrP^{C}) into the β–sheet-rich, aggregated, toxic and protease-resistant conformer (PrP^{Sc}) is the central event in the pathogenesis of TSE. However, despite many years of research, the pathogenic mechanism of structural change and which parts of prion participate in this conversion process are still unclear. In our previous study, we found that the disulfide bond-removed PrP can spontaneously proceed structural conversion under native condition and can immediately become β structure in higher salt concentration. This finding provided an ideal model for studying structure conversion of prion protein under the native condition. The thesis here is aimed to explore the role of three alpha-helices on the structural conversion of mouse prion protein. The results can be divided into three parts: the structural information about spontaneous structural conversion, β-PrP oligomers and fibrils, respectively.

In the first part, the disulfide bond-removed PrP, D147C and Q217C carried out spontaneous structural conversion under native condition by CD spectroscopy (fig. 4.1). By ESR technique with the usage of nanopores, we also observed the spontaneous structural transition process of recombinant full-length prion protein with time (fig. 4.3). These results further confirmed our previous notion that disulfide bond is essential to

prion protein stability and reduction of disulfide bond may be important for structural conversion in vivo. However, in order to provide ideal ESR signals, we used high protein concentration (0.45 mM) which was 100-fold times higher than the concentration used for CD experiments. Such high protein concentration may accelerate protein conversion and parts of PrP would immediately become β structure (fig. 4.2). Only S132R1 with lower concentration (0.27 mM) showed predominant α structure. Despite this, we can still observe that ESR spectra changed after 2 weeks measurements (fig. 4.3). In ESR spectra, fast component had increased with time, indicating that conformation dynamic of PrP might increase during structural conversion. In contrast, information about specific residue was imaged in slow component. Slow component of S132R1 was not affected by time, suggesting that this residue might not be involved in the conversion process. For D147R1, slow component had slightly increased during the experiment, indicating that residue 147 might be partially involved in the structural conversion. Furthermore, Q217R1 showed inter-spin interaction at the beginning and the interaction had increased gradually with time, implying that residue 217 may have involved in association process. According to the high intensity of slow component, residue 217 is in a more ordered state. All these data are consistent with the following ESR spectra of β-PrP oligomers. However, the slow component of N181R1 did not increase as the way we expected.

N181R1 may need more time to aggregate. In addition, pH value is important to structural conversion of disulfide bond removed PrP. The conversion rate slowed down at a more acid condition (fig. 4.4 & 4.5). Even previous paper had suggested that PrP oligomers formed immediately in an acid condition (Bocharova et al, 2005). It should be noted that their PrP contained disulfide bond and was existed in a more acid condition (pH < 5) with denaturant.

In the second part, D147C and Q217C can immediately become β structure at a higher salt condition (fig. 4.6). The same as the previous study, AUC results (fig. 4.7) and TEM images (fig. 4.8) both confirmed that β-PrP was oligomers form, and the β-PrP also showed high ThT-binding ability (fig. 4.9). ESR spectra provided the supporting evidence that the local environment of four different residues proceeded in oligomerization.(fig. 4.11). The ESR spectra of S132R1 indicated that residue-132 in soluble β-PrP remained highly flexibility, implying that it may not involve in the β-PrP oligomers formation. D147R1 and N181R1 both contained slow and fast ESR spectral components, which indicated that helix 1 and helix 2 possibly become partially unfolded during the β-PrP oligomers formation. Spin labeled on helix 3 showed slow mobility, suggesting that the local environment of residue 217 is in an ordered state. Moreover, no regular spin-spin distance could be found in the β-PrP by CW-ESR

(distance detection range <20 Å). Interestingly, PrP oligomers can further form amyloid fibrils at RT without shaking (fig. 4.10). However, in all previous studies, formation of amyloid fibrils was performed in denaturing agents; even the fibrils which generated under native-like condition was incubated under acid condition (Cobb et al, 2008). We confirmed that the disulfide bond removed PrP can form not only oligomers but also fibrils under the native condition without denaturant. Furthermore, ThT intensity did not increased after forming amyloid fibrils. These results suggested that our β-PrP oligomer may be an on-pathway intermediate for fibril formation.

In the third part, we transformed the mutant PrP into fibril structure under a partially denaturing condition. The lag time of mutant PrP was all shorter then $mPrP^{wt}$, suggesting that disulfide bond-deleted PrP are easier to form amyloid seed (fig. 4.12). Furthermore, MTSSL-labeling did not affect the lag time and the fibrillization ability of mutant PrP (fig 4.14). However, R1 group on residue 181 might interferes the association between monomer and existing fibrils based on the prolonged elongation rate. The morphology of different amyloid fibrils was similar except the mutant on Q217 producing more twisted structure (fig. 4.13 and fig. 4.15). ESR technique combined with pepsin digestion assay was used to study the amyloid structure. The ESR spectra of fibrils formed from S132R1 and D147R1 were more flexible than from

N181R1 and Q217R1 which both showed broaden signals (fig. 4.16). Inter-spin interaction disappeared in the spectrum of S132R1 fibrils after pepsin treatment, suggesting that the residue 132 may exist in a flexible region in fibril structure. On the other hand, the spectra of other sites remained to show substa ntial inter-spin interactions after the pepsin treatment, indicating that these residues are not affected by pepsin digestion and may not exposed in the fibril structure. However, residue 181 is one of the N-glycosylation sites of PrP^C in vivo, so it may not be involved in the amyloid core. Based on ESR spectra and ThT assay, N181 is possible near the amyloid core in the fibril structure. Moreover, the ESR spectra of Q217R1 fibrils showed intermolecular spin interaction with a distance of 10 Å. Therefore, helix 3 becomes regular arrangement with small intermolecular distance in amyloid fibril. Our ESR spectra are consistent with the previous report which proposed that amyloid core region is located at residues 160–220 (Cobb et al, 2007). However, we observed that all fibrils became shorter not thinner after pepsin digestion (fig. 4.17). This was not expectable because limited proteolysis should remove the peripheral residues without interfering fibrils association. A recent report suggested that His residues were protonated in an acidic condition and leaded to charge repulsion which further caused the dissociation of prion fibrils (Qi et al, 2012). Therefore, pepsin is not the ideal protease to study prion fibrils because it needs an acidic condition.

Overall, residue 132 maintains its flexibility no matter in spontaneous transition, β-PrP oligomers or amyloid fibrils, suggesting this residue may not participate in structural conversion. Yet, the solid-state NMR of human prion peptide 124-147 proposed that this region became in-register parallel β-sheet (Lin et al, 2010). Therefore, residue 132 may be located at the loop region between β-strands or this region is not change during structural conversion. Helix 1 and helix 2 likely become partially unfolded in β-PrP oligomers. And residue 147 is more exposed than residue 181 while forming amyloid fibrils. We suggested that residue 147 and 181 may not involve in amyloid core. On the other hand, helix 3 is compactable in spontaneous structural conversion, β-PrP oligomers and amyloid fibrils. And residue 217 has short intermolecular distance (10 Å) in amyloid fibril. Moreover, the fibril morphology becomes differently according to the residue 217 mutation. These data indicate that helix 3 may be important in association, but whether it is involved in the amyloid core or still in helical structure remains further studies.

Chapter 6 Future Works

In the future, there are many problems needed to be solved and required more experiments to clarify the structural conversion mechanism of prion protein. For example, the distance change during structural conversion can be measured by adding two labels on helix 3 combined with ESR or FRET techniques. If the distance is unchanged, which means that helix 3 is remained in helical structure and vice versa. Alternatively, supposing that helix 3 is involved in amyloid core, fibrils formed from helix 3 peptide should be able to seed wildtype prion protein by decreasing the lag time of fibrillization and, wildtype fibrils should be able to seed helix 3 peptides as well. In addition, more mutation sites are necessary for further study. For instance, spin labeled on residue 135 or 137 can assure that whether regions 124-147 are involved in amyloid core or not. Moreover, for limited limited proteolysis assay, proteinase K is a better choice because of pepsin is not an ideal protease for prion fibrils. We also have to further adjust ESR experiments about spontaneous structural conversion. ESR experiment needs high protein concentration but this will accelerate PrP aggregation. To solve this problem, we can dissolve PrP in a more acidic condition which slows down the conversion rate, so we may get more proper information. On the other hand, pulsed ESR technique may provide intermolecular distance for PrP samples which cannot be detected by CW-ESR.

References

Aguzzi A, Sigurdson C, Heikenwalder M (2007) Molecular mechanisms of prion pathogenesis. *Annu Rev Pathol-Mech* **3:** 11-40

Alper T, Cramp WA, Haig DA, Clarke MC (1967) Does the agent of scrapie replicate without nucleic acid? *Nature* **214:** 764-766

Alper T, Haig DA, Clarke MC (1966) The exceptionally small size of the scrapie agent. *Biochem Biophys Res Commun* **22:** 278-284

Anfinsen CB (1973) Principles that govern the folding of protein chains. *Science* **181:** 223-230

Baskakov IV, Legname G, Baldwin MA, Prusiner SB, Cohen FE (2002) Pathway complexity of prion protein assembly into amyloid. *J Biol Chem* **277:** 21140-21148

Bendheim PE, Brown HR, Rudelli RD, Scala LJ, Goller NL, Wen GY, Kascsak RJ, Cashman NR, Bolton DC (1992) Nearly ubiquitous tissue distribution of the scrapie agent precursor protein. *Neurology* **42:** 149

Bocharova OV, Breydo L, Parfenov AS, Salnikov VV, Baskakov IV (2005) In vitro conversion of full-length mammalian prion protein produces amyloid form with physical properties of PrP(Sc). *J Mol Biol* **346:** 645-659

Bremer J, Baumann F, Tiberi C, Wessig C, Fischer H, Schwarz P, Steele AD, Toyka KV, Nave K-A, Weis J, Aguzzi A (2010) Axonal prion protein is required for peripheral myelin maintenance. *Nat Neurosci* **13:** 310-318

Brown DR, Qin K, Herms JW, Madlung A, Manson J, Strome R, Fraser PE, Kruck T, von Bohlen A, Schulz-Schaeffer W, Giese A, Westaway D, Kretzschmar H (1997) The cellular prion protein binds copper in vivo. *Nature* **390:** 684-687

Bruce ME, Will RG, Ironside JW, McConnell I, Drummond D, Suttie A, McCardle L, Chree A, Hope J, Birkett C, Cousens S, Fraser H, Bostock CJ (1997) Transmissions to mice indicate that `new variant' CJD is caused by the BSE agent. *Nature* **389:** 498-501

Bueler H, Aguzzi A, Sailer A, Greiner RA, Autenried P, Aguet M, Weissmann C (1993)

Mice devoid of PrP are resistant to scrapie. *Cell* **73:** 1339-1347

Bueler H, Fischer M, Lang Y, Bluethmann H, Lipp H-P, DeArmond SJ, Prusiner SB, Aguet M, Weissmann C (1992) Normal development and behaviour of mice lacking the neuronal cell-surface PrP protein. *Nature* **356:** 577-582

Burns CS, Aronoff-Spencer E, Dunham CM, Lario P, Avdievich NI, Antholine WE, Olmstead MM, Vrielink A, Gerfen GJ, Peisach J, Scott WG, Millhauser GL (2002) Molecular features of the copper binding sites in the octarepeat domain of the prion protein. *Biochemistry* **41:** 3991-4001

Castilla J, Saá P, Hetz C, Soto C (2005) In vitro generation of infectious scrapie prions. *Cell* **121:** 195-206

Caughey B, Baron GS (2006) Prions and their partners in crime. *Nature* **443:** 803-810

Chaudhary YS, Manna SK, Mazumdar S, Khushalani D (2008) Protein encapsulation into mesoporous silica hosts. *Micropor Mesopor Mat* **109:** 535-541

Cobb NJ, Apetri AC, Surewicz WK (2008) Prion protein amyloid formation under native-like conditions involves refolding of the C-terminal alpha-helical domain. *J Biol Chem* **283:** 34704-34711

Cobb NJ, Sonnichsen FD, McHaourab H, Surewicz WK (2007) Molecular architecture of human prion protein amyloid: a parallel, in-register beta-structure. *Proc Natl Acad Sci U S A* **104:** 18946-18951

Cobb NJ, Surewicz WK (2009) Prion diseases and their biochemical mechanisms. *Biochemistry* **48:** 2574-2585

Collinge J (2001) Prion diseases of humans and animals: their causes and molecular basis. *Annu Rev Neurosci* **24:** 519-550

Collinge J, Whittington MA, Sidle KCL, Smith CJ, Palmer MS, Clarke AR, Jefferys JGR (1994) Prion protein is necessary for normal synaptic function. *Nature* **370:** 295-297

Cooke JA, Brown LJ (2011) Distance measurements by continuous wave EPR

spectroscopy to monitor protein folding. *Methods Mol Biol* **752:** 73-96

Criado JR, Sánchez-Alavez M, Conti B, Giacchino JL, Wills DN, Henriksen SJ, Race R, Manson JC, Chesebro B, Oldstone MBA (2005) Mice devoid of prion protein have cognitive deficits that are rescued by reconstitution of PrP in neurons. *Neurobiol Dis* **19:** 255-265

Cuille J, Chelle P-L (1939) Transmission experimental de la tremblante chez la chevre. *C R Acad Sci* **208:** 1058-1060

Davies P, Brown DR (2008) The chemistry of copper binding to PrP: is there sufficient evidence to elucidate a role for copper in protein function? *Biochem J* **410:** 237-244

DeMarco ML, Daggett V (2004) From conversion to aggregation: protofibril formation of the prion protein. *Proc Natl Acad Sci U S A* **101:** 2293-2298

Frare E, Mossuto MF, Polverino de Laureto P, Dumoulin M, Dobson CM, Fontana A (2006) Identification of the core structure of lysozyme amyloid fibrils by proteolysis. *J Mol Biol* **361:** 551-561

Gajdusek DC, Gibbs CJ, Alpers M (1966) Experimental transmission of a Kuru-like syndrome to chimpanzees. *Nature* **209:** 794-796

Gibbs CJ, Jr., Gajdusek DC, Asher DM, Alpers MP, Beck E, Daniel PM, Matthews WB (1968) Creutzfeldt-Jakob disease (spongiform encephalopathy): transmission to the chimpanzee. *Science* **161:** 388-389

Govaerts C, Wille H, Prusiner SB, Cohen FE (2004) Evidence for assembly of prions with left-handed β-helices into trimers. *Proc Natl Acad Sci U S A* **101:** 8342-8347

Griffith JS (1967) Self-replication and scrapie. *Nature* **215:** 1043-1044

Hadlow WJ (1959) Scrapie and Kuru. *Lancet* **ii:** 289-290

Hafner-Bratkovic I, Bester R, Pristovsek P, Gaedtke L, Veranic P, Gaspersic J, Mancek-Keber M, Avbelj M, Polymenidou M, Julius C, Aguzzi A, Vorberg I, Jerala R (2011) Globular domain of the prion protein needs to be unlocked by domain swapping to support prion protein conversion. *J Biol Chem* **286:** 12149-12156

Hammes GG (2005) Principles of nuclear magnetic resonance and electron spin resonance. In *Spectroscopy for the Biological Sciences*, pp 103-128. John Wiley & Sons, Inc.

Helmus JJ, Surewicz K, Nadaud PS, Surewicz WK, Jaroniec CP (2008) Molecular conformation and dynamics of the Y145Stop variant of human prion protein in amyloid fibrils. *Proc Natl Acad Sci* **105:** 6284-6289

Hooper NM (1990) Proteolytic enzymes: a practical approach edited by R J Beynon and J S Bond. pp 259. IRL Press at Oxford University Press, Oxford. 1989. £29 (spiral bound)/£19 (paper) ISBN 0-19-963058-5/963059-3. *Biochemical Education* **18:** 55-55

Hsiao K, Scott M, Foster D, Groth D, DeArmond S, Prusiner S (1990) Spontaneous neurodegeneration in transgenic mice with mutant prion protein. *Science* **250:** 1587-1590

Huang YW, Chiang YW (2011) Spin-label ESR with nanochannels to improve the study of backbone dynamics and structural conformations of polypeptides. *Phys Chem Chem Phys* **13:** 17521-17531

Hubbell WL, Altenbach C (1994) Investigation of structure and dynamics in membrane proteins using site-directed spin labeling. *Curr Opin Struct Biol* **4:** 566-573

Imran M, Mahmood S (2011) An overview of animal prion diseases. *Virol J* **8:** 493

Jackson GS, Hosszu LL, Power A, Hill AF, Kenney J, Saibil H, Craven CJ, Waltho JP, Clarke AR, Collinge J (1999) Reversible conversion of monomeric human prion protein between native and fibrilogenic conformations. *Science* **283:** 1935-1937

Jarrett JT, Lansbury PT, Jr. (1993) Seeding "one-dimensional crystallization" of amyloid: a pathogenic mechanism in Alzheimer's disease and scrapie? *Cell* **73:** 1055-1058

Kanaani J, Prusiner SB, Diacovo J, Baekkeskov S, Legname G (2005) Recombinant prion protein induces rapid polarization and development of synapses in embryonic rat hippocampal neurons in vitro. *J Neurochem* **95:** 1373-1386

Kleschyov AL, Wenzel P, Munzel T (2007) Electron paramagnetic resonance (EPR) spin trapping of biological nitric oxide. *J Chromat B, Analyt Technol Biomed Life Sci* **851:** 12-20

Knaus KJ, Morillas M, Swietnicki W, Malone M, Surewicz WK, Yee VC (2001) Crystal structure of the human prion protein reveals a mechanism for oligomerization. *Nat Struct Mol Biol* **8:** 770-774

Kretzschmar HA, Prusiner SB, Stowring LE, DeArmond SJ (1986) Scrapie prion proteins are synthesized in neurons. *Am J Pathol* **122:** 1-5

Kumar J, Sreeramulu S, Schmidt TL, Richter C, Vonck J, Heckel A, Glaubitz C, Schwalbe H (2010) Prion protein amyloid formation involves structural rearrangements in the C-terminal domain. *ChemBioChem* **11:** 1208-1213

López García F, Zahn R, Riek R, Wüthrich K (2000) NMR structure of the bovine prion protein. *Proc Natl Acad Sci* **97:** 8334-8339

Langedijk JP, Fuentes G, Boshuizen R, Bonvin AM (2006) Two-rung model of a left-handed beta-helix for prions explains species barrier and strain variation in transmissible spongiform encephalopathies. *J Mol Biol* **360:** 907-920

Lee S-W, Mou Y, Lin S-Y, Chou F-C, Tseng W-H, Chen C-h, Lu C-YD, Yu SSF, Chan JCC (2008) Steric zipper of the amyloid fibrils formed by residues 109–122 of the syrian hamster prion protein. *J Mol Biol* **378:** 1142-1154

Lin NS, Chao JC, Cheng HM, Chou FC, Chang CF, Chen YR, Chang YJ, Huang SJ, Chan JC (2010) Molecular structure of amyloid fibrils formed by residues 127 to 147 of the human prion protein. *Chemistry* **16:** 5492-5499

Lisa Washmon-Kriel VLJ, Kenneth J. Balkus Jr. (2000) Cytochrome c immobilization into mesoporous molecular sieves. *J Mol Catal B-enzym* **10:** 453-469

Longhi S, Belle V, Fournel A, Guigliarelli B, Carriere F (2011) Probing structural transitions in both structured and disordered proteins using site-directed spin-labeling EPR spectroscopy. *J Pept Sci* **17:** 315-328

Lu X, Wintrode PL, Surewicz WK (2007) Beta-sheet core of human prion protein

amyloid fibrils as determined by hydrogen/deuterium exchange. *Proc Natl Acad Sci U S A* **104:** 1510-1515

Lysek DA, Schorn C, Nivon LG, Esteve-Moya V, Christen B, Calzolai L, von Schroetter C, Fiorito F, Herrmann T, Guntert P, Wuthrich K (2005) Prion protein NMR structures of cats, dogs, pigs, and sheep. *Proc Natl Acad Sci USA* **102:** 640-645

Málaga-Trillo E, Solis GP, Schrock Y, Geiss C, Luncz L, Thomanetz V, Stuermer CAO (2009) Regulation of embryonic cell adhesion by the prion protein. *PLoS Biol* **7:** e1000055

M.P. Hornshaw JRM, and J.M. Candy (1995) Copper binding to the N-terminal tandem repeat regions of mammalian and avain prion protein. *Biochem Biophys Res Commun* **207:** 621-629

Makarava N, Baskakov IV (2008) Expression and purification of full-length recombinant PrP of high purity. *Methods Mol Biol* **459:** 131-143

McKinley MP, Bolton DC, Prusiner SB (1983) A protease-resistant protein is a structural component of the scrapie prion. *Cell* **35:** 57-62

Morillas M, Vanik DL, Surewicz WK (2001) On the Mechanism of α-Helix to β-Sheet Transition in the Recombinant Prion Protein†. *Biochemistry* **40:** 6982-6987

Nelson R, Sawaya MR, Balbirnie M, Madsen AO, Riekel C, Grothe R, Eisenberg D (2005) Structure of the cross-β spine of amyloid-like fibrils. *Nature* **435:** 773-778

Oesch B, Westaway D, Walchli M, McKinley MP, Kent SB, Aebersold R, Barry RA, Tempst P, Teplow DB, Hood LE, et al. (1985) A cellular gene encodes scrapie PrP 27-30 protein. *Cell* **40:** 735-746

Pan K, Baldwin M, Nguyen J, Gasset M, Serban A, Groth D, Mehlhorn I, Huang Z, Fletterick R, Cohen F, Prusiner S (1993) Conversion of α-helices β-sheets features in the formation of the scrapie prion proteins. *Proc Natl Acad Sci USA* **90:** 10962-10966

Perini F, Vidal R, Ghetti B, Tagliavini F, Frangione B, Prelli F (1996) PrP27–30 is a normal soluble prion protein fragment released by human platelets. *Biochem Biophys Res Commun* **223:** 572-577

Prusiner S (1991) Molecular biology of prion diseases. *Science* **252:** 1515-1522

Prusiner SB (1982) Novel proteinaceous infectious particles cause scrapie. *Science* **216:** 136-144

Prusiner SB (1998) Prions. *Proc Natl Acad Sci U S A* **95:** 13363-13383

Qi X, Moore RA, McGuirl MA (2012) Dissociation of recombinant prion protein fibrils into short protofilaments: implications for the endocytic pathway and involvement of the N-terminal domain. *Biochemistry*

Riek R, Hornemann S, Wider G, Billeter M, Glockshuber R, Wuthrich K (1996) NMR structure of the mouse prion protein domain PrP(121-231). *Nature* **382:** 180-182

Rogers NG, Basnight M, Gibbs CJ, Gajdusek DC (1967) Latent viruses in chimpanzees with experimental kuru. *Nature* **216:** 446-449

Ryou C (2011) Prion diseases. In *eLS*. John Wiley & Sons, Ltd

Sawaya MR, Sambashivan S, Nelson R, Ivanova MI, Sievers SA, Apostol MI, Thompson MJ, Balbirnie M, Wiltzius JJW, McFarlane HT, Madsen AO, Riekel C, Eisenberg D (2007) Atomic structures of amyloid cross-β spines reveal varied steric zippers. *Nature* **447:** 453-457

Spielhaupter C, Schätzl HM (2001) PrPC directly interacts with proteins involved in signaling pathways. *J Biol Chem* **276:** 44604-44612

Stahl N, Baldwin MA, Teplow DB, Hood L, Gibson BW, Burlingame AL, Prusiner SB (1993) Structural studies of the scrapie prion protein using mass spectrometry and amino acid sequencing. *Biochemistry* **32:** 1991-2002

Steadman LB (1980) Ethnology: Kuru sorcery: disease and danger in the New Guinea Highlands. Shirley Lindenbaum. *Am Anthropol* **82:** 692-694

Surewicz WK, Apostol MI (2011) Prion protein and its conformational conversion: a structural perspective. *Top Curr Chem* **305:** 135-167

Swietnicki W, Morillas M, Chen SG, Gambetti P, Surewicz WK (1999) Aggregation and fibrillization of the recombinant human prion protein huPrP90−231. *Biochemistry* **39:** 424-431

Trevitt CR, Singh PN (2003) Variant Creutzfeldt-Jakob disease: pathology, epidemiology, and public health implications. *Am J Clin Nutr* **78:** 651S-656S

Tycko R, Savtchenko R, Ostapchenko VG, Makarava N, Baskakov IV (2010) The α-Helical C-Terminal Domain of Full-Length Recombinant PrP Converts to an In-Register Parallel β-Sheet Structure in PrP Fibrils: Evidence from Solid State Nuclear Magnetic Resonance. *Biochemistry* **49:** 9488-9497

Walsh P, Simonetti K, Sharpe S (2009) Core structure of amyloid fibrils formed by residues 106–126 of the human prion protein. *Structure* **17:** 417-426

Wang F, Wang X, Yuan C-G, Ma J (2010) Generating a prion with bacterially expressed recombinant prion protein. *Science* **327:** 1132-1135

Wasmer C, Lange A, Van Melckebeke H, Siemer AB, Riek R, Meier BH (2008) Amyloid fibrils of the HET-s(218–289) prion form a β solenoid with a triangular hydrophobic core. *Science* **319:** 1523-1526

Wells G, Scott A, Johnson C, Gunning R, Hancock R, Jeffrey M, Dawson M, Bradley R (1987) A novel progressive spongiform encephalopathy in cattle. *Vet Rec* **121:** 419-420

Wilesmith J, Ryan J, Atkinson M (1991) Bovine spongiform encephalopathy: epidemiological studies on the origin. *Vet Rec* **128:** 199-203

Will RG (2003) Acquired prion disease: iatrogenic CJD, variant CJD, kuru. *Br Med Bull* **66:** 255-265

Will RG, Ironside JW, Zeidler M, Cousens SN, Estibeiro K, Alperovitch A, Poser S, Pocchiari M, Hofman A, Smith PG (1996) A new variant of Creutzfeldt-Jakob disease in the UK. *Lancet* **347:** 921-925

Wille H, Bian W, McDonald M, Kendall A, Colby DW, Bloch L, Ollesch J, Borovinskiy AL, Cohen FE, Prusiner SB, Stubbs G (2009) Natural and synthetic prion structure from X-ray fiber diffraction. *Proc Natl Acad Sci* **106:** 16990-16995

Wille H, Michelitsch MD, Guénebaut V, Supattapone S, Serban A, Cohen FE, Agard DA, Prusiner SB (2002) Structural studies of the scrapie prion protein by electron crystallography. *Proc Natl Acad Sci* **99:** 3563-3568